ELSEVIER

Comput. Methods Appl. Mech. Engrg. 183 (2000) 331–352

Computer methods in applied mechanics and engineering

www.elsevier.com/locate/cma

Anisotropic damage in quasi-brittle solids: modelling, computational issues and applications

A. Dragon *, D. Halm, Th. Désoyer

Laboratoire de Mécanique et de Physique des Matériaux, CNRS and ENSMA, Poitiers-Futuroscope, 86960 Futuroscope Cedex, France

Received 6 April 1998

Abstract

Crucial issues concerning non-linear behaviour of quasi-brittle materials like some rocks, concrete and certain ceramics are addressed in the paper. In fact, inelastic response for this class of solids results from the evolution of a large number of micro- and mesocracks accompanied with frictional effects regarding closed cracks for compressive loading paths. Progressive microcracking produces volumetric dilatancy, induced anisotropy and further pressure sensitivity on the macroscale.

A continuum damage model attempting to capture salient features of progressive anisotropic degradation and accounting for frictional sliding over internal crack surfaces is synthesised. The model is three-dimensional and micro-mechanically motivated in its essential ingredients. At the same time it is built to provide a tool for structural analysis purpose. The settlement between apparently conflicting requirements of physical pertinency on the one hand and of applicability of the model on the other, is endeavoured through relative simplicity of the approach (a small number of material constants to identify) and its modular character allowing three distinct degrees of complexity.

The first 'basic' level concerns modelling of the anisotropic degradation by multiple mesocrack growth generating volumetric dilatancy and non-symmetrical strength effects. The second level consists in accounting for the "normal" moduli recovery with respect to mesocrack-sets constrained to close under predominantly compressive loads (unilateral effect). The damage and frictional blocking/sliding coupled effects are dealt with in a non-classical way at the third level allowing thus to treat highly complex loading paths with rotating loading and damage axes (torsional paths for example). Hysteretic effects for loading and unloading due to plasticity-like mesocrack friction are commented.

Some computational aspects relative to the model (in its basic, extended and coupled version) are then outlined. It is stressed that a fully implicit integration scheme appears naturally compatible one for a class of damage models as it is for the model at stake (in spite of its specific features). The frictional sliding evolution is dealt with in a way close to plasticity integration algorithms. Concomitant growth of damage and frictional sliding is successfully managed by coupled algorithm. The corresponding double integration is facilitated by low interaction degree between damage and sliding criteria.

Significant examples are shown illustrating damage and friction induced non-linear behaviour together with complex hysteretic effects for cyclic loading. They illustrate relevancy of the coupled model for quasi-brittle rocks and efficiency of the algorithms employed.

1. Introduction

Some important issues concerning inelastic behaviour of quasi-brittle solids (e.g. rock-like materials) are explored and modelled in this paper in the framework of rate-type constitutive theory with internal variables. It is well confirmed nowadays that the non-linear response in such solids under loading results from the evolution of multiple internal micro- and mesocrack-like defects generating progressive degradation of moduli associated with secondary anisotropy effects, volumetric dilatancy and other events. Opening and closure of microcrack-sets under varying loads lead to further complex phenomena like recovery of some

* Corresponding author.

0045-7825/00/$ - see front matter
PII: S0045-7825(99)00225-X

degraded moduli in the direction perpendicular to closed crack systems and frictional blocking and/or sliding over the internal crack surfaces.

Recently an interesting tentative of a global vision of the non-linear mechanics of materials has been proposed by Lubarda and Krajcinovic [1], including the classical rate theory of elastoplastic deformation of crystalline solids as well as the non-linear framework for progressively mesofracturing solids. Indeed, even for the latter class of quasi-brittle materials, the continuum damage approach attempting to capture progressive degradation attributable to evolution of multiple defects should be coupled with the plasticity-like approach accounting for irreversible frictional sliding over the internal crack surfaces. The extended framework of damage-elastoplastic constitutive models allows for study of complex, cyclic and non-proportional loading paths, where coupled microcrack-growth and friction related dissipative mechanisms produce strong non-linearity, induced anisotropy and intricate hysteresis.

When considering progressively mesofracturing solid under compressive loadings, i.e. with some crack-sets constrained to closure the initial unloading process is frequently friction-locked, exhibiting a high apparent rigidity. Further unloading may be dissipative if reverse multistage frictional sliding (reverse with respect to a loading branch) becomes active. The inelastic unloading is just a particular effect revealing the above-mentioned coupling of damage by microcracking with a form of plasticity generated by frictional sliding on closed cracks. A strong evidence in this sense can be found for example in Walsh [2].

The problem received some attention in the past in regard to modelling, see e.g. [3–9], and very recently, [10]. For the most part the texts adduced represent pertinent micromechanical studies leading, for some of them, to models capable to cover a limited range of stress–strain paths (two-dimensional, axisymmetric, etc.). The purpose of this paper is to address, in a synthetic manner, basic issues of the 3D-modelling proposed by the present authors, employing an internal variable formalism for the joint process of anisotropic damage by microcracking and frictional sliding at closed microcracks. The aim of this model is to provide an efficient, macroscopic – whereas strongly micromechanically motivated – approach suitable for boundary-value problems involving non-linear behaviour of quasi-brittle solids.

The approach presented is based on an anisotropic damage model, the "basic version", proposed by Dragon [11] and extended by Halm and Dragon [12] to include the unilateral effect concerning normal stiffness recovery with respect to a mesocrack system constrained to closure. This extended version, summarized in Section 2, is then completed by the damage and frictional blocking/sliding model depicted above. The coupled model allows to treat complex loading paths with eventually rotating loading and damage axes. The corresponding developments are given in Sections 3 and 4. Besides, a somewhat elementary presentation of the coupled model is given in Ref. [13] by Halm and Dragon. Here, an overview covering the three modular segments of the model, i.e. the basic version and the extended one, treated together in Section 2, and the coupled damage-and-friction model completed in Section 4, is presented. The aim here is to set forth a more general survey including a methodology relative to the numerical integration of the constitutive equations proposed. The numerical schemes employed, respectively for the damage model, for the mesocrack-friction plasticity and for the coupled model are given in Section 5. Some selected examples illustrating damage and friction induced non-linear stress–strain behaviour, together with hysteretic effects, are furthermore presented and commented in this section.

The crucial issue of the control of microcrack closure and opening phenomena is addressed through Sections 2–4, where the stiffness recovery and friction enter into consideration. The central simplifying hypothesis, conveyed through the developments proposed, consists in reduction of any real microcrack-set configuration to an equivalent configuration of three mutually orthogonal systems of parallel cracks characterized by three eigenvectors $\boldsymbol{v}^k$ $(k=1, 2, 3)$ and three non-negative eigenvalues D_k of the second-order damage tensor $\boldsymbol{D}$. In such a manner the damage-induced anisotropy is systematically limited to a form of orthotropy, see also [14].

The problem of transition from volume-distributed damage to surface-localized failure incipience has been amply debated at the end of eighties and the beginning of nineties, see for example [15–17]. The localization bifurcation in the presence of damage by microcracking inducing net anisotropy effects needs clearly a 3D treatment, two-dimensional projections misrepresenting mostly localization mechanisms (orientation and discontinuity mode). The computational procedure relative to 3D localization detection is given in Ref. [11], where some pertinent results obtained with the basic damage model are amply commented.

2. Anisotropic damage and normal unilateral effect

This section outlines the salient features of the anisotropic damage model by Dragon [11], Halm and Dragon [12], which forms the framework for further developments presented in Sections 3 and 4. An objective of the damage model summarized below is to describe – in a realistic manner applicable to structural calculus – the process of mesocrack-induced anisotropic degradation and relative behaviour of an elastic rock-like 'quasi-brittle' solid. It stipulates evaluation of effective elastic moduli of a material with microcracks and an adequate description of the evolution of damage. The emphasis has been put on an "open" formulation of the model to allow further extensions and couplings. It is based on the hypotheses and developments ordered below in the items from (i) to (v):

(i) A single damage internal variable is constituted by a symmetric, second-order tensor $\boldsymbol{D}$ indicating orientation of microcrack set(s) as well as the dissipative mechanism under consideration, namely generation and growth of decohesion microsurfaces:

$$\boldsymbol{D} = \sum_i d^i(s)\, \boldsymbol{n}^i \otimes \boldsymbol{n}^i. \tag{1}$$

The scalar density $d^i(s)$ is proportional to the extent s of decohesion surface and the unit normal vector $\boldsymbol{n}^i$ describes orientation of the ith set of parallel crack-like defects. The form (1) is motivated by micromechanical considerations (see, e.g. [3,14]) but in the context further on here the density $d(s)$ is reckoned as a macroscopic quantity. The expression (1) is in itself a guiding microstructural interpretation of damage-related internal variable $\boldsymbol{D}$. Since $\boldsymbol{D}$ is a symmetric second-order tensor it has three positive eigenvalues D_k ($k=1,\ 2,\ 3$) and three orthogonal eigenvectors $\boldsymbol{v}^k$. This means that any system of microcracks (1), decomposed into $1,\ldots,\ i,\ldots,\ n$ of subsystems of parallel mesocracks can be reduced to three equivalent orthogonal sets of cracks characterized by densities D_k and normal vectors $\boldsymbol{v}^k$

$$\boldsymbol{D} = \sum_{k=1}^{3} D_k\, \boldsymbol{v}^k \otimes \boldsymbol{v}^k. \tag{2}$$

(ii) The damage-dependent strain energy (free energy per unit volume) $w(\boldsymbol{\varepsilon}, \boldsymbol{D})$ generates a form of elastic orthotropy – in connection to the three eigensystems (2) – for $\boldsymbol{D} \neq \boldsymbol{0}$; w is assumed a linear function of $\boldsymbol{D}$ and in this way corresponding to non-interacting cracks hypothesis. On the other hand, it contains linear and quadratic terms in $\boldsymbol{\varepsilon}$. A particular invariant form given below (formula (4)) comprises a single linear term reading $g\ \mathrm{tr}(\boldsymbol{\varepsilon}\cdot\boldsymbol{D})$, g is a constant, corresponding to damage-induced residual phenomena. The damage induced macroscopic residual stress for $\boldsymbol{\varepsilon}=\boldsymbol{0}$ is thus explicitly obtained equal to $g\boldsymbol{D}$. Inversely, for $\boldsymbol{\sigma}=\boldsymbol{0}$, non-zero residual strain is induced.

(iii) Under predominantly compressive loading, favourably oriented cracks close leading to an elastic moduli recovery phenomenon in the direction normal to the closed cracks. It is called here normal unilateral effect – in the absence of frictional sliding (the latter, when accounted for later, will induce a 'shear' recovery effect as well) – and requires more involved damage characterization. In fact, for a set of cracks constrained against opening a fourth-order tensorial density is necessary for a rigorous, micromechanically motivated description. A compromise solution has been advanced in [12] between micromechanical considerations imposing an additional fourth-order damage variable and macroscopic modelling efficiency. The formulation maintains the orthotropy of the effective, elastic properties – instead of eventual more general anisotropy induced by a new fourth-order damage tensor – and the complementary fourth-order entity $\hat{\boldsymbol{D}}$, necessary to account for the normal unilateral effect, is directly assembled with the eigenvalues and eigenvectors of $\boldsymbol{D}$ and cannot therefore be considered as a new damage internal variable:

$$\hat{\boldsymbol{D}} = \sum_{k=1}^{3} D_k\, \boldsymbol{v}^k \otimes\ \boldsymbol{v}^k \otimes \boldsymbol{v}^k \otimes \boldsymbol{v}^k. \tag{3}$$

(iv) A single scalar simultaneous invariant of $\hat{\boldsymbol{D}}$ and $\boldsymbol{\varepsilon}$, namely $\boldsymbol{\varepsilon} : \hat{\boldsymbol{D}} : \boldsymbol{\varepsilon}$, completes the expression of the free energy $w[\boldsymbol{\varepsilon},\ \boldsymbol{D},\ \hat{\boldsymbol{D}}(\boldsymbol{D})]$ (thermodynamic potential), with no additional material constant with respect to the basic form $w(\boldsymbol{\varepsilon}, \boldsymbol{D})$ postulated in (ii). Rigorous continuity analysis in the framework of multilinear

elasticity (for a given damage state), recast in [12], leads to a simple microcrack closure condition for an equivalent set, namely: $\boldsymbol{v}^k \cdot \boldsymbol{\varepsilon} \cdot \boldsymbol{v}^k \leqslant 0$. The detailed expression of $w(\boldsymbol{\varepsilon}, \boldsymbol{D})$ including the supplementary term allowing for normal unilateral effect is:

$$w(\boldsymbol{\varepsilon}, \boldsymbol{D}) = \frac{1}{2}\lambda(\operatorname{tr}\boldsymbol{\varepsilon})^2 + \mu \operatorname{tr}(\boldsymbol{\varepsilon}\cdot\boldsymbol{\varepsilon}) + g \operatorname{tr}(\boldsymbol{\varepsilon}\cdot\boldsymbol{D}) + \alpha \operatorname{tr}\boldsymbol{\varepsilon} \operatorname{tr}(\boldsymbol{\varepsilon}\cdot\boldsymbol{D}) + 2\beta \operatorname{tr}(\boldsymbol{\varepsilon}\cdot\boldsymbol{\varepsilon}\cdot\boldsymbol{D}) - (\alpha+2\beta)\boldsymbol{\varepsilon} : \left[\sum_{k=1}^{3} H(-\boldsymbol{v}^k\cdot\boldsymbol{\varepsilon}\cdot\boldsymbol{v}^k) D_k \boldsymbol{v}^k \otimes \boldsymbol{v}^k \otimes \boldsymbol{v}^k \otimes \boldsymbol{v}^k\right] : \boldsymbol{\varepsilon}, \tag{4}$$

where H is the classical Heaviside function; α, β are material constants related to modified elastic moduli for a given damage state. λ and μ are conventional Lamé constants for elastic (non-damaged) solid matrix.

The corresponding damage-induced orthotropic elasticity representation $\boldsymbol{\sigma}(\boldsymbol{\varepsilon}, \boldsymbol{D})$ and the damage driving (thermodynamic) force $\boldsymbol{F}^{\mathrm{D}}$ are determined by corresponding partial derivation:

$$\boldsymbol{\sigma} = \frac{\partial w}{\partial \boldsymbol{\varepsilon}} = \lambda(\operatorname{tr}\boldsymbol{\varepsilon})\mathbf{1} + 2\mu\boldsymbol{\varepsilon} + g\boldsymbol{D} + \alpha[\operatorname{tr}(\boldsymbol{\varepsilon}\cdot\boldsymbol{D})\mathbf{1} + (\operatorname{tr}\boldsymbol{\varepsilon})\boldsymbol{D}] + 2\beta(\boldsymbol{\varepsilon}\cdot\boldsymbol{D} + \boldsymbol{D}\cdot\boldsymbol{\varepsilon}) - 2(\alpha+2\beta)\sum_{k=1}^{3} H(-\boldsymbol{v}^k\cdot\boldsymbol{\varepsilon}\cdot\boldsymbol{v}^k) D_k(\boldsymbol{v}^k\cdot\boldsymbol{\varepsilon}\cdot\boldsymbol{v}^k)\boldsymbol{v}^k\otimes\boldsymbol{v}^k, \tag{5}$$

$$\boldsymbol{F}^{\mathrm{D}} = -\frac{\partial w}{\partial \boldsymbol{D}} = -g\boldsymbol{\varepsilon} - \alpha(\operatorname{tr}\boldsymbol{\varepsilon})\boldsymbol{\varepsilon} - 2\beta(\boldsymbol{\varepsilon}\cdot\boldsymbol{\varepsilon}) + (\alpha+2\beta)\sum_{k=1}^{3} H(-\boldsymbol{v}^k\cdot\boldsymbol{\varepsilon}\cdot\boldsymbol{v}^k)\cdot(\boldsymbol{v}^k\cdot\boldsymbol{\varepsilon}\cdot\boldsymbol{v}^k)^2\boldsymbol{v}^k\otimes\boldsymbol{v}^k. \tag{6}$$

In spite of the presence of the Heaviside function $H(-\boldsymbol{v}^k\cdot\boldsymbol{\varepsilon}\cdot\boldsymbol{v}^k)$, w, $\boldsymbol{\sigma}$ and $\boldsymbol{F}^{\mathrm{D}}$ remain continuous when passing from the open mesocracks configuration to the closed mesocracks configuration and vice versa.

(v) The evolution of $\boldsymbol{D}$, corresponding to the brittle, splitting-like crack kinetics, has been found to follow the normality rule with respect to a criterion in the space of components of the proper thermodynamic force (affinity) $\boldsymbol{F}^{\mathrm{D}}$. The damage evolution is thus apparently following the principle of maximum (damage) dissipation, see also [18], and is related here to tensile (positive) straining $\boldsymbol{\varepsilon}^+$ and to actual damage pattern. It should be stressed however that the particular damage criterion $f(\boldsymbol{F}^{\mathrm{D}}, \boldsymbol{D}) \leqslant 0$ is explicitly dependent on the part $\boldsymbol{F}^{\mathrm{D1+}} = -g\boldsymbol{\varepsilon}^+ = \boldsymbol{F}^{\mathrm{D}} - \boldsymbol{F}^{\mathrm{D2}} - \boldsymbol{F}^{\mathrm{D1-}}$ of the driving force $\boldsymbol{F}^{\mathrm{D}}$. $\boldsymbol{F}^{\mathrm{D1}}$ is the strain energy release rate term related to residual 'locked' effects : $\boldsymbol{F}^{\mathrm{D1}} = -g\boldsymbol{\varepsilon}$, $\boldsymbol{F}^{\mathrm{D2}}$ represents the remaining recoverable energy release rate. The former term is decomposed into the splitting part $\boldsymbol{F}^{\mathrm{D1+}} = -g\boldsymbol{\varepsilon}^+$, $\boldsymbol{\varepsilon}^+ = \boldsymbol{P}^+ : \boldsymbol{\varepsilon}$, with $\boldsymbol{P}^+$ a positive fourth-order projection operator selecting positive eigenvalues from strain, and the non-splitting part $\boldsymbol{F}^{\mathrm{D1-}} = -g(\boldsymbol{\varepsilon} - \boldsymbol{\varepsilon}^+)$. The damage criterion and rate-independent damage evolution law are thus as follows:

$$f(\boldsymbol{F}^{\mathrm{D}} - \boldsymbol{F}^{D2} - \boldsymbol{F}^{\mathrm{D1-}}; \boldsymbol{D}) = \sqrt{\frac{1}{2}\operatorname{tr}\left[(\boldsymbol{F}^{\mathrm{D}} - \boldsymbol{F}^{\mathrm{D2}} - \boldsymbol{F}^{\mathrm{D1-}})\cdot(\boldsymbol{F}^{\mathrm{D}} - \boldsymbol{F}^{\mathrm{D2}} - \boldsymbol{F}^{\mathrm{D1-}})\right]} + B\operatorname{tr}\left[(\boldsymbol{F}^{\mathrm{D}} - \boldsymbol{F}^{\mathrm{D2}} - \boldsymbol{F}^{\mathrm{D1-}})\cdot\boldsymbol{D}\right] - (C_0 + C_1 \operatorname{tr}\boldsymbol{D}) \leqslant 0, \tag{7}$$

$$\dot{\boldsymbol{D}} = \Lambda_D \frac{\partial f}{\partial \boldsymbol{F}^{\mathrm{D}}} = \begin{cases} 0 & \text{if } f < 0 \quad \text{or} \quad f = 0,\ \dot{f} < 0 \\ \Lambda_D\left[\dfrac{\boldsymbol{\varepsilon}^+}{\sqrt{2\operatorname{tr}(\boldsymbol{\varepsilon}^+\cdot\boldsymbol{\varepsilon}^+)}} + \boldsymbol{B}\boldsymbol{D}\right] & \text{if } f = 0 \quad \text{and} \quad \dot{f} = 0; \end{cases} \qquad \Lambda_D \geqslant 0. \tag{8}$$

Remarks: The damage criterion (7) transferred to stress-space (see [11,12]) represents a strongly pressure-sensitive surface with a marked dissymmetry of traction vs. compression limits.

The fourth-order tensor $\dot{\boldsymbol{D}}$ depends entirely on $\boldsymbol{D}$ (see definition (3)); it does not require a separate evolution law.

In numerical calculations any loading path is considered as a collection of $\boldsymbol{D}$-proportional segments. The form of Eq. (6) is valid for such a segment, i.e. for a given configuration of principal directions of $\boldsymbol{D}$. Otherwise it should be completed to account for a novel configuration of the tensor $\dot{\boldsymbol{D}}$.

The model, non-linear as it is, contains eight material constants only: λ, μ, α, β, g, B, C_0 and C_1, which can be relatively easily determined (see Section 5.2).

In order to illustrate the predictive capacities of the model, the curves in Fig. 1 show the stress–strain behaviour according to the basic model and experiment (Pecqueur et al. [19]) for Vosges sandstone submitted to axisymmetric triaxial compression with a confining pressure $P_c = 15$ MPa. The set of material

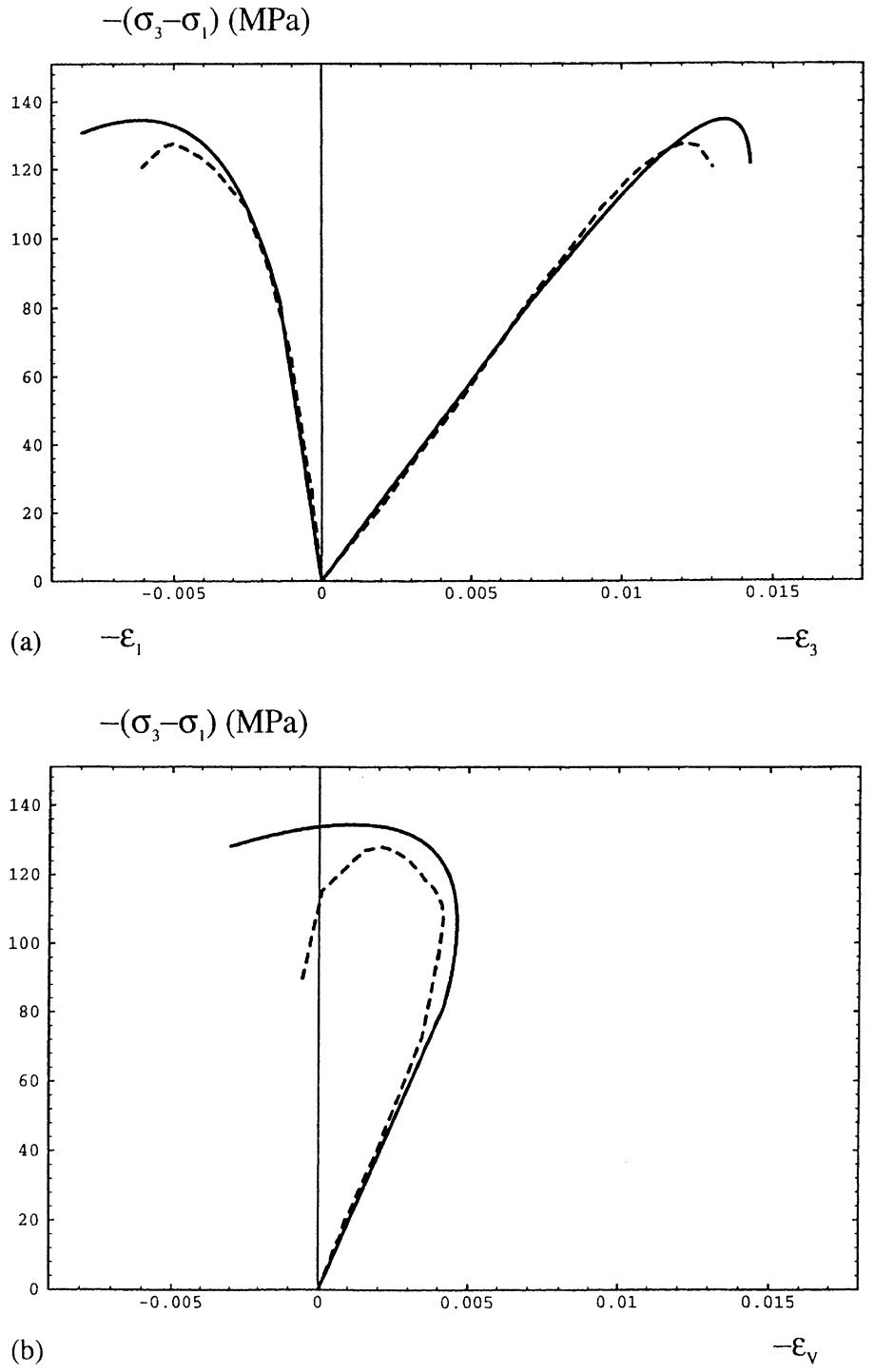

Fig. 1. Comparison simulation (solid line) vs. experiment (dashed line) for a triaxial compression (confining ressure $P_c = 15$ MPa) on Vosges sandstone. (a) deviatoric stress $-(\sigma_3 - \sigma_1)$ vs. axial $-\varepsilon_3$ and transversal $-\varepsilon_1$ strain. (b) deviatoric stress $-(\sigma_3 - \sigma_1)$ vs. volumetric strain $-\varepsilon_V$.

constants, namely $\lambda = 3250$ MPa, $\mu = 4875$ MPa, $\alpha = 9925$ MPa, $\beta = -11180$ MPa, $g = -32$ MPa, $C_0 = 0.02$ MPa, $C_1 = 0.27$ MPa, $B = 0$, was determined according to the procedure described in Section 5.2. The dilatancy effect resulting from pronounced damage is well evidenced in Fig. 1(b). The numerical simulations conform to experimental programme correspond to homogeneous stress–strain paths realized at a single Gauss point. For the location of bifurcation point with respect to stress–strain peak for a large spectrum of axisymmetric stress–strain paths, see [11].

While the curves in Fig. 1 correspond to a routine experimental test for rock-like solids, the lateral overloading sequence following the foregoing compression test is much less common and needs somewhat sophisticated equipment. Three simulations of lateral overloading for previously damaged solid are shown in Fig. 2. The reference strain $\boldsymbol{\varepsilon}_1^{A,B,C}$ corresponds to the lateral strain value at the beginning of step c. The stiffness recovery occurring during overloading (step c) has been calculated following the extended model presented above accounting for the unilateral, crack-closure related behaviour, see [12] for further details. Three successive simulations were performed for different values of the axial peak stress $|\boldsymbol{\sigma}_3|_{\max}$, i.e. for different damage values corresponding to reduced moduli represented by initial segments in Fig. 2(c).

An operational, structural analysis approach employing the concept of damage should combine an efficient damage model implemented in robust computer algorithm associated with proper tools for detection and control of bifurcation phenomena. The latter indicate eventual transition from distributed damage to surface-like localization considered as a precursor of macroscopic fracture. In any case bifurcation events point out an ill-posedness of the problem and necessity of remaking a computational scheme. Actually, the basic model presented, i.e. the one summarized above *except* the last, unilateral effect related term in $w(\boldsymbol{\varepsilon}, \boldsymbol{D})$, see Eq. (4) and counterparts in (5) and (6), was extensively tested for its capacities to generate physically sound localized failure mechanisms, see, e.g. [11]. Essential structure of the numerical scheme employed for the 3D localization detection and some notable results obtained with the basic damage model are summarized in the latter paper. The very fair predictions concerning the localization bifurcation obtained for homogeneous stress–strain paths as well as for boundary-value problems related to rock engineering applications have prompted further developments of the model itself including its coupling with a form of mesocrack-friction-induced plasticity as put forward in the next section.

3. Mesocrack friction induced plasticity

The unilateral normal effect included in the model summarized in Section 2 allows a moduli recovery in the direction normal to the closed mesocracks. It fails to capture a shear moduli recovery in the direction parallel to the crack plane, resulting from some blocking of mesocrack lips displacement due to roughness and corresponding friction phenomena. Experimental data involving loading–unloading cycles for specimens subjected to torsion and hydrostatic compression for instance show hysteretic effects generated by such a blocking and subsequent frictional sliding on closed mesocrack lips. The beginning of unloading is characterized by a quasi-vertical curve while further decreasing slope is linked to progressive sliding, see for example [20]. Some attempts of micromechanical modelling of the phenomena deserve attention, [3–10]. However they are not directly operational for an efficient structural analysis. Some of earlier attempts (Kachanov [3], Horii and Nemat-Nasser [4]) consider the influence of friction on effective moduli but do not provide satisfactory thermodynamic interpretation of sliding evolution. Most of existing approaches are limited to two-dimensional analyses, as e.g. [7], with the notable exception of the more recent work by Gambarotta and Lagomarsino [8].

3.1. Elastic-damage and friction response

The global strain expression for a representative volume of elastic solid of stiffness $\boldsymbol{C}$ containing microcracks (assumed plane and quasi-circular for simplicity) can be written as a sum of the solid matrix contribution $\boldsymbol{\varepsilon}^0$ and the crack contribution $\boldsymbol{\varepsilon}^c$:

$$\boldsymbol{\varepsilon} = \boldsymbol{C}^{-1} : \boldsymbol{\sigma} + \frac{1}{2V}\sum_i (\langle \boldsymbol{b} \rangle \otimes \boldsymbol{n} + \boldsymbol{n} \otimes \langle \boldsymbol{b} \rangle)^i s^i = \boldsymbol{\varepsilon}^0 + \sum_i \boldsymbol{\varepsilon}^{ci} \tag{9}$$

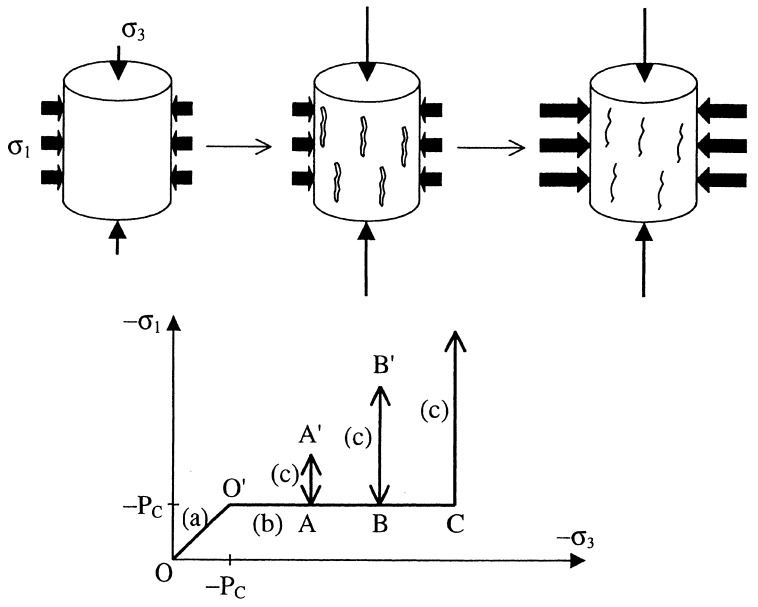

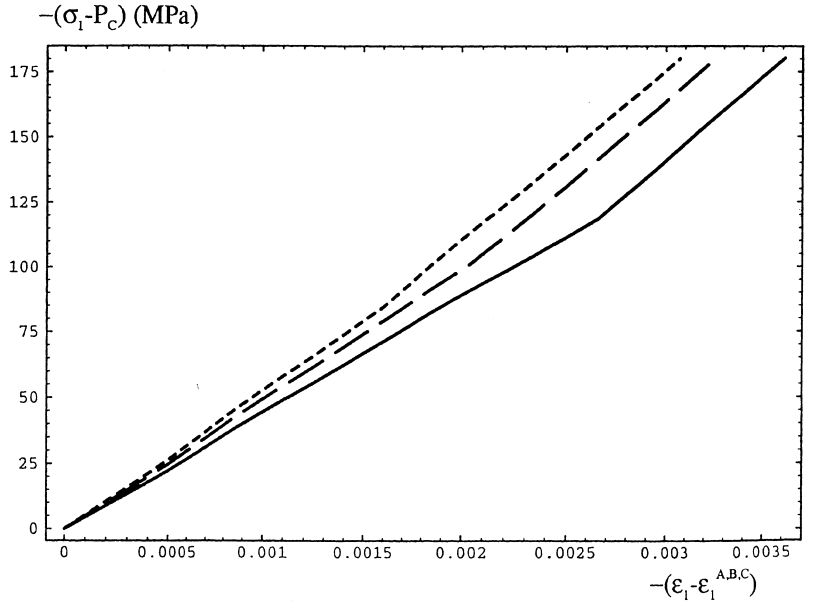

Fig. 2. Triaxial compression with lateral overloading: loading paths and simulated lateral stress $-(\sigma_3 - P_c)$ vs. lateral strain $-(\varepsilon_1 - \varepsilon_1^{A,B,C})$ for Fontainebleau sandstone.

with the crack displacement discontinuity $\boldsymbol{b}^i$ being averaged ($\langle \boldsymbol{b}^i \rangle$) for the microcrack set i. For closed sliding cracks, as long as the orientation $\boldsymbol{n}^i$ is preserved, $\langle \boldsymbol{b}^i \rangle$ is orthogonal to $\boldsymbol{n}^i$:

$$\langle \boldsymbol{b}^i \rangle = \xi^i \boldsymbol{g}^i, \quad \boldsymbol{g}^i \perp \boldsymbol{n}^i \quad \text{if } \boldsymbol{n}^i = \text{const.} \tag{10}$$

with ξ^i representing the amount of sliding in the direction $\boldsymbol{g}^i$. One can write furthermore:

$$\boldsymbol{\varepsilon}^{ci} = \frac{s^i}{2V} \xi^i (\boldsymbol{g}^i \otimes \boldsymbol{n}^i + \boldsymbol{n}^i \otimes \boldsymbol{g}^i). \tag{11}$$

Hence, for the microcrack system i, the sliding variable is chosen in the form:

$$\boldsymbol{\gamma}^i = \frac{s^i\ \xi^i}{V}\,\mathrm{sym}(\boldsymbol{n}\otimes\boldsymbol{g})^i \tag{12}$$

the symmetrisation being operated for the expression in parentheses. The similarity with (1) is striking: as for $\boldsymbol{D}$, the form of $\boldsymbol{\gamma}$ is motivated by micromechanics; as for $d(s)$ the quantity $s^i\xi^i/V$ cannot be explicitly calculated in the framework of a macroscopic model. Moreover, as any system of microcracks represented by $\boldsymbol{D}$ reduces to three equivalent sets according to (2), the sliding tensor $\boldsymbol{\gamma}$ can be written in the analogous manner:

$$\boldsymbol{\gamma} = \sum_{k=1}^{3}\frac{s^k\,\xi^k}{V}\,\mathrm{sym}(\boldsymbol{v}\otimes\boldsymbol{g})^k = \sum_{k=1}^{3}\boldsymbol{\gamma}^k,$$

where $\boldsymbol{v}^k,\ k=1,\ 2,\ 3$ are $\boldsymbol{D}$-eigenvectors.

Let us consider, for a while, a single system of mesocracks characterized by the only principal non-zero component D_3 and the normal (eigenvector) $\boldsymbol{v}^3$. The objective here is to argue for an enlarged form of the free-energy function $w(\boldsymbol{\varepsilon};\boldsymbol{D},\boldsymbol{\gamma})$ accounting for the frictional blocking and sliding effects for closed crack sets.

From (4) and (5) one can infer that the anisotropic damage-induced shear moduli are entirely determined by μ (solid matrix shear modulus) and the term $2\beta\ \mathrm{tr}(\boldsymbol{\varepsilon}\cdot\boldsymbol{\varepsilon}\cdot\boldsymbol{D})$. Hence, for the damage configuration at stake ($D_1=D_2=0;\ D_3\neq 0$) one obtains:

$$\sigma_{13} = 2\mu\varepsilon_{13} + 2\beta D_3\varepsilon_{13}, \qquad \sigma_{23} = 2\mu\varepsilon_{23} + 2\beta D_3\varepsilon_{23}.$$

The degradation of moduli in the normal direction to the open crack set is described in the *conjugate* manner by the α-term as well as the β-one. The expression of the Young modulus E_3 for the damage configuration as above is

$$E_3 = \lambda + 2\mu + 2\alpha D_3 + 4\beta D_3 - \frac{(\lambda+\alpha D_3)^2}{\lambda+\mu}.$$

Let us consider the transition from open cracks to closed ones, assuming friction resistant lips when in contact. The crack-open form of (4), with $H(-\boldsymbol{v}^3\cdot\boldsymbol{\varepsilon}\cdot\boldsymbol{v}^3)=0$ applies for the former case. When the cracks are closed and blocked by friction resistance at a given $\boldsymbol{\gamma}$, the shear modulus μ is recovered and this should be properly reflected in the new modified expression $w(\boldsymbol{\varepsilon};\boldsymbol{D},\boldsymbol{\gamma})$. The β-term should be counterbalanced in this expression. The α-term, having no influence on shear moduli, enters as before. Additional invariants including $\boldsymbol{\gamma}$ can be only simultaneous ($\boldsymbol{\gamma}$, $\boldsymbol{D}$)-invariants as there is no sliding on crack lips in the absence of damage. As from (12) one infers $\mathrm{tr}\,\boldsymbol{\gamma}=0$ and $\mathrm{tr}(\boldsymbol{\gamma}\cdot\boldsymbol{D})=0$ (for conservative damage axes), only two simultaneous invariants of $\boldsymbol{\varepsilon}$, $\boldsymbol{\gamma}$ and $\boldsymbol{D}$ convey useful information. They are: $\mathrm{tr}\,(\boldsymbol{\varepsilon}\cdot\boldsymbol{\gamma}\cdot\boldsymbol{D})$ and $\mathrm{tr}(\boldsymbol{\gamma}\cdot\boldsymbol{\gamma}\cdot\boldsymbol{D})$. The argument for the quantity including β in the last term of (4) was to restitute the normal stiffness reduced by the term $2\beta\mathrm{tr}\ (\boldsymbol{\varepsilon}\cdot\boldsymbol{\varepsilon}\cdot\boldsymbol{D})$ in the first line of (4), but since this latter term is going to be counterbalanced, the former quantity has to disappear from w. Doing so allows one to write the expression $w(\boldsymbol{\varepsilon};\boldsymbol{D},\boldsymbol{\gamma})$ for closed friction-resistant crack lips in the form (for a single crack system):

$$\begin{aligned} w(\boldsymbol{\varepsilon},\boldsymbol{D},\boldsymbol{\gamma}) = {} & \frac{1}{2}\lambda(\mathrm{tr}\,\boldsymbol{\varepsilon})^2 + \mu\,\mathrm{tr}(\boldsymbol{\varepsilon}\cdot\boldsymbol{\varepsilon}) + g\,\mathrm{tr}(\boldsymbol{\varepsilon}\cdot\boldsymbol{D}) + \alpha\,\mathrm{tr}\,\boldsymbol{\varepsilon}\,\mathrm{tr}(\boldsymbol{\varepsilon}\cdot\boldsymbol{D}) - \alpha(\boldsymbol{\varepsilon}:\hat{\boldsymbol{D}}:\boldsymbol{\varepsilon}) + \eta_1\,\mathrm{tr}(\boldsymbol{\varepsilon}\cdot\boldsymbol{\gamma}\cdot\boldsymbol{D}) \\ & + 2\eta_2\,\mathrm{tr}(\boldsymbol{\gamma}\cdot\boldsymbol{\gamma}\cdot\boldsymbol{D}), \end{aligned} \tag{13}$$

where η_1 and η_2 are material constants to be identified.

From the micromechanics viewpoint there are infinity of crack-closure paths possible (straight, slantwise, mixed,...). The macroscopic model continuity requires continuity for expressions of $w(\boldsymbol{\varepsilon};\boldsymbol{D},\boldsymbol{\gamma})$ and $\boldsymbol{\sigma}$ for crack opening-to-closure (and reverse) transition. This leads to the following condition at the closure-point:

$$\begin{cases} \boldsymbol{\varepsilon}\cdot\boldsymbol{D} = \boldsymbol{\gamma}\cdot\boldsymbol{D} \\ \boldsymbol{D}\cdot\boldsymbol{\varepsilon} = \boldsymbol{D}.\boldsymbol{\gamma} \end{cases} \iff \gamma_{ij} = \mathrm{sym}(\varepsilon_{ik}v_k v_j) \quad \text{at closure-point.} \tag{14}$$

The latter formula constitutes an initialization for the sliding variable $\boldsymbol{\gamma}$ and can be explained as follows: at closure point, the sliding quantity $\boldsymbol{\gamma}$ is equal to the strain $\boldsymbol{\varepsilon}$ in the crack plane, the matrix transmits its deformation to the crack.

According to the continuity conditions for multilinear elasticity (Wesolowski [21], Curnier et al. [22]) already employed in [12] in the context of unilateral normal effect, see Eqs. (4)–(6) Section 2, the jump of effective elastic stiffness $[[\boldsymbol{C}^*]]$ between open crack (the corresponding energy is designated by w^0 below) and closed crack respective configurations should be a singular operator. It is sufficient that its all second-order determinants be equal to zero.

In the present context – Eq. (13) at the very closure point, taking into account (14) – $[[\boldsymbol{C}^*]]$ is given as follows:

$$[[\boldsymbol{C}^*]] = \left.\frac{\partial^2 w}{\partial\boldsymbol{\varepsilon}\partial\boldsymbol{\varepsilon}}\right|_{\gamma,D} - \left.\frac{\partial^2 w^0}{\partial\boldsymbol{\varepsilon}\partial\boldsymbol{\varepsilon}}\right|_{D}; \quad [[C^*_{ijkl}]] = \left(\frac{1}{2}\eta_1 + \eta_2 - \beta\right)\left(\delta_{ik}\,D_{jl} + \delta_{jl}\,D_{ik} + \delta_{il}\,D_{jk} + \delta_{jk}\,D_{il}\right) - 2\alpha\hat{D}_{ijkl}.$$

The above-mentioned singularity requirement and the additional stronger condition allowing no stress jump in the strain space across the surface $\boldsymbol{v}\cdot\boldsymbol{\varepsilon}\cdot\boldsymbol{v} = 0$, applied by Halm and Dragon [13] (in the way similar as in [12]) lead, respectively to:

$$\begin{aligned} &\frac{1}{2}\eta_1 + \eta_2 - \beta = 0 \\ &\eta_1 = 4\beta. \end{aligned} \tag{15}$$

The free-energy $w(\boldsymbol{\varepsilon};\boldsymbol{D},\boldsymbol{\gamma})$ can now be written as follows (for either open or closed cracks):

$$\begin{aligned} w(\boldsymbol{\varepsilon};\boldsymbol{D},\boldsymbol{\gamma}) = {}& \frac{1}{2}\lambda(\operatorname{tr}\varepsilon)^2 + \mu\,\operatorname{tr}(\boldsymbol{\varepsilon}\cdot\boldsymbol{\varepsilon}) + g\,\operatorname{tr}(\boldsymbol{\varepsilon}\cdot\boldsymbol{D}) + \alpha\,\operatorname{tr}\boldsymbol{\varepsilon}\,\operatorname{tr}(\boldsymbol{\varepsilon}\cdot\boldsymbol{D}) + 2\beta\,\operatorname{tr}(\boldsymbol{\varepsilon}\cdot\boldsymbol{\varepsilon}\cdot\boldsymbol{D}) \\ &+ H(-\boldsymbol{v}\cdot\boldsymbol{\varepsilon}\cdot\boldsymbol{v})[-\alpha\boldsymbol{\varepsilon}:\hat{\boldsymbol{D}}:\boldsymbol{\varepsilon} - 2\beta\,\operatorname{tr}(\boldsymbol{\varepsilon}\cdot\boldsymbol{\varepsilon}\cdot\boldsymbol{D}) + 4\beta\,\operatorname{tr}(\boldsymbol{\varepsilon}\cdot\boldsymbol{\gamma}\cdot\boldsymbol{D}) - 2\beta\,\operatorname{tr}(\boldsymbol{\gamma}\cdot\boldsymbol{\gamma}\cdot\boldsymbol{D})]. \end{aligned} \tag{16}$$

The expression (16) can be generalized to three non-interactive equivalent crack sets represented by eigenvectors $\boldsymbol{v}^{\mathrm{k}}$ associated with the principal components D_k, $k=1, 2, 3$. One can select the kth set using the following projection operator $\boldsymbol{L}^k$:

$$\begin{aligned} &\boldsymbol{L}^k = \boldsymbol{v}^k\otimes\boldsymbol{v}^k\otimes\boldsymbol{v}^k\otimes\boldsymbol{v}^k \\ &\boldsymbol{D}^k = D_k\boldsymbol{v}^k\otimes\boldsymbol{v}^k = \boldsymbol{L}^k:\boldsymbol{D}. \end{aligned} \tag{17}$$

This allows to write counterpart equations of (4)–(6) independently for each equivalent set, all possible configurations being included (open or closed, sliding or non-sliding sets):

$$\begin{aligned} w(\boldsymbol{\varepsilon},\boldsymbol{D},\boldsymbol{\gamma}) = {}& \frac{1}{2}\lambda(\operatorname{tr}\boldsymbol{\varepsilon})^2 + \mu\,\operatorname{tr}(\boldsymbol{\varepsilon}\cdot\boldsymbol{\varepsilon}) + g\,\operatorname{tr}(\boldsymbol{\varepsilon}\cdot\boldsymbol{D}) + \alpha\,\operatorname{tr}\boldsymbol{\varepsilon}\,\operatorname{tr}(\boldsymbol{\varepsilon}\cdot\boldsymbol{D}) + 2\beta\,\operatorname{tr}(\boldsymbol{\varepsilon}\cdot\boldsymbol{\varepsilon}\cdot\boldsymbol{D}) \\ &+ \sum_{k=1}^{3} H(-\boldsymbol{v}^k\cdot\boldsymbol{\varepsilon}\cdot\boldsymbol{v}^k)\big[-\alpha\boldsymbol{\varepsilon}:(\boldsymbol{D}_k\,\boldsymbol{L}^k):\boldsymbol{\varepsilon} - 2\beta\,\operatorname{tr}(\boldsymbol{\varepsilon}\cdot\boldsymbol{\varepsilon}\cdot\boldsymbol{D}^k) + 4\beta\,\operatorname{tr}(\boldsymbol{\varepsilon}\cdot\boldsymbol{\gamma}^k\cdot\boldsymbol{D}^k) \\ &- 2\beta\,\operatorname{tr}(\boldsymbol{\gamma}^k\cdot\boldsymbol{\gamma}^k\cdot\boldsymbol{D}^k)\big], \end{aligned} \tag{18}$$

$$\begin{aligned} \boldsymbol{\sigma} = \frac{\partial w}{\partial\boldsymbol{\varepsilon}} = {}& \lambda(\operatorname{tr}\boldsymbol{\varepsilon})\mathbf{1} + 2\mu\boldsymbol{\varepsilon} + g\boldsymbol{D} + \alpha[\operatorname{tr}(\boldsymbol{\varepsilon}\cdot\boldsymbol{D})\mathbf{1} + (\operatorname{tr}\boldsymbol{\varepsilon})\boldsymbol{D}] + 2\beta(\boldsymbol{\varepsilon}\cdot\boldsymbol{D} + \boldsymbol{D}\cdot\boldsymbol{\varepsilon}) \\ &+ \sum_{k=1}^{3} H(-\boldsymbol{v}^k\cdot\boldsymbol{\varepsilon}\cdot\boldsymbol{v}^k)\big[-2\alpha D_k(\boldsymbol{v}^k\cdot\boldsymbol{\varepsilon}\cdot\boldsymbol{v}^k)\boldsymbol{v}^k\otimes\boldsymbol{v}^k - 2\beta(\boldsymbol{\varepsilon}\cdot\boldsymbol{D}^k + \boldsymbol{D}^k\cdot\boldsymbol{\varepsilon}) \\ &+ 2\beta(\boldsymbol{\gamma}^k\cdot\boldsymbol{D}^k + \boldsymbol{D}^k\cdot\boldsymbol{\gamma}^k)\big], \end{aligned} \tag{19}$$

$$\begin{aligned} \boldsymbol{F}^{\mathrm{D}} = -\frac{\partial w}{\partial\boldsymbol{D}} = {}& -g\boldsymbol{\varepsilon} - \alpha(\operatorname{tr}\boldsymbol{\varepsilon})\boldsymbol{\varepsilon} - 2\beta(\boldsymbol{\varepsilon}\cdot\boldsymbol{\varepsilon}) \\ &+ \sum_{k=1}^{3}\boldsymbol{H}(-\boldsymbol{v}^k\cdot\boldsymbol{\varepsilon}\cdot\boldsymbol{v}^k)\Big[\alpha(\boldsymbol{v}^k\cdot\boldsymbol{\varepsilon}\cdot\boldsymbol{v}^k)^2\boldsymbol{v}^k\otimes\boldsymbol{v}^k + 2\beta\boldsymbol{L}^k:(\boldsymbol{\varepsilon}\cdot\boldsymbol{\varepsilon}) - 4\beta\boldsymbol{L}^k:(\boldsymbol{\varepsilon}\cdot\boldsymbol{\gamma}^k) + 2\beta\boldsymbol{L}^k:(\boldsymbol{\gamma}^k\cdot\boldsymbol{\gamma}^k)\Big]. \end{aligned} \tag{20}$$

As each equivalent set of the normal $\boldsymbol{v}^k$ is to be considered independently, the corresponding affinity (thermodynamic force) is:

$$\boldsymbol{F}^{\gamma k} = -\frac{\partial w}{\partial \boldsymbol{\gamma}^k} = H(-\boldsymbol{v}^k \cdot \boldsymbol{\varepsilon} \cdot \boldsymbol{v}^k)\big[-2\beta(\boldsymbol{\varepsilon} \cdot \boldsymbol{D}^k + \boldsymbol{D}^k \cdot \boldsymbol{\varepsilon}) + 2\beta(\boldsymbol{\gamma}^k \cdot \boldsymbol{D}^k + \boldsymbol{D}^k \cdot \boldsymbol{\gamma}^k)\big]. \tag{21}$$

The remark concerning Eq. (6), Section 2, stating its validity for a $\boldsymbol{D}$-proportional segment, i.e. for a given configuration of principal direction of $\boldsymbol{D}$, is still in force for Eq. (20).

3.2. Sliding criterion and evolution

The model herein considers frictional non-sliding/sliding phenomena on mesocrack lips on a macroscopic scale, by an approach similar to that to damage, notwithstanding the micromechanical background and interpretations of $\boldsymbol{D}$ and γ. So, the Coulomb criterion form, function of the corresponding shear and normal tractions on a crack lip, employed in micromechanical models (Horii and Nemat-Nasser [4], Andrieux et al. [7], Gambarotta and Lagomarsino [8]), is methodologically less suitable in the present context. The pertinent thermodynamic affinity governing frictional sliding on an equivalent system k, ($k = 1, 2, 3$) is the entity $\boldsymbol{F}^{\gamma k}$ defined above as the strain energy release-rate with respect to $\boldsymbol{\gamma}^k$.

The frictional non-sliding/sliding complementary law is based on the hypotheses as follows:

(i) The sliding criterion depends explicitly on the norm of the tangential part $\boldsymbol{F}^{\gamma Tk}$ of the 'force' $\boldsymbol{F}^{\gamma k}$ and on the normal strain $\boldsymbol{v}^k \cdot \boldsymbol{\varepsilon} \cdot \boldsymbol{v}^k$ consecutively to the strain-related representation of the energy w and the crack-closure criterion at stake ($\boldsymbol{v}^k \cdot \boldsymbol{\varepsilon} \cdot \boldsymbol{v}^k \leqslant 0$).

(ii) Contrarily to inconsistencies relative to the normality rule in the classical Coulomb framework affected by appearance of a normal separating velocity (cf. for example [23,24]) a standard scheme in the space of forces conjugate to $\boldsymbol{\gamma}^k$ keeps physical pertinence. The normality rule appears to relate the frictional sliding rate to the tangential force $\boldsymbol{F}^{\gamma Tk}$ indicating its leaning to the crack plane (for a $\boldsymbol{D}^k$-proportional loading segment).

Consequently, the corresponding convex reversibility domain $h^k \leqslant 0$ can be written as:

$$h^k\big(\boldsymbol{F}^{\gamma k} - \boldsymbol{F}^{\gamma Nk}, \boldsymbol{v}^k \cdot \boldsymbol{\varepsilon} \cdot \boldsymbol{v}^k\big) = \sqrt{\frac{1}{2}\quad \mathrm{tr}\big[\big(\boldsymbol{F}^{\gamma k} - \boldsymbol{F}^{\gamma Nk}\big)\big(\boldsymbol{F}^{\gamma k} - \boldsymbol{F}^{\gamma Nk}\big)\big]} + \rho \boldsymbol{v}^k \cdot \boldsymbol{\varepsilon} \cdot \boldsymbol{v}^k \leqslant 0 \quad \text{if } \boldsymbol{v}^k \cdot \boldsymbol{\varepsilon} \cdot \boldsymbol{v}^k \leqslant 0, \tag{22}$$

where ρ is a material constant, a strain-related friction coefficient in the space ($\boldsymbol{F}^{\gamma k}$, $\boldsymbol{\varepsilon}$) and

$$\boldsymbol{F}^{\gamma k} = \boldsymbol{F}^{\gamma Tk} + \boldsymbol{F}^{\gamma Nk}; \quad \boldsymbol{F}^{\gamma Tk} = \boldsymbol{F}^{\gamma k} - (\boldsymbol{v}^k \cdot \boldsymbol{F}^{\gamma k} \cdot \boldsymbol{v}^k)\, \boldsymbol{v}^k \otimes \boldsymbol{v}^k; \quad \boldsymbol{F}^{\gamma \mathrm{Nk}} = (\boldsymbol{v}^k \cdot \boldsymbol{F}^{\gamma k} \cdot \boldsymbol{v}^k)\, \boldsymbol{v}^k \otimes \boldsymbol{v}^k. \tag{23}$$

The normality rule for $\dot{\boldsymbol{\gamma}}^k$ is then

$$\dot{\boldsymbol{\gamma}}^k = \Lambda_\gamma^{\mathrm{k}} \frac{\partial h^k(\boldsymbol{F}^{\gamma k} - \boldsymbol{F}^{\gamma Nk}, \boldsymbol{v}^k \cdot \boldsymbol{\varepsilon} \cdot \boldsymbol{v}^k)}{\partial \boldsymbol{F}^{\gamma k}} = \begin{cases} 0 & \text{if } h^k < 0 \quad \text{or} \quad h^k = 0, \dot{h}^k < 0 \\ \Lambda_\gamma^k \dfrac{\boldsymbol{F}^{\gamma Tk}}{\sqrt{2\mathrm{tr}(\boldsymbol{F}^{\gamma Tk} \cdot \boldsymbol{F}^{\gamma \mathrm{Tk}})}} & \text{if } h^k = 0 \quad \text{and} \quad \dot{h}^k = 0, \Lambda_\gamma^k \geqslant 0. \end{cases} \tag{24}$$

Detailed comments on salient aspects of the criterion $h^k = 0$ in the strain space are given by Halm and Dragon [13]. Fig. 3 shows the corresponding form together with a hardening-like phenomenon (for $\boldsymbol{\gamma}^k \neq 0$) in reduced stress space (σ_{33}, σ_{13}). The similitude between the actual yield surface and the Coulomb one can be clearly noticed. In connection with the crack opening/closure condition (a single crack system $D_3 \neq 0$ is considered for illustration) the cone $h^k = 0$ is shifted to the left: it corresponds to negative value of σ_{33} at the closure point.

By examining the complete set (18)–(24) of the equations of the model, one can see that the frictional sliding does not sweep away the relative simplicity of the enlarged model (see the end of Section 2). Only one additional constant ρ adds to eight material constants (λ, μ, α, β, C_0, C_1, g, B). It can be stressed that ρ governs the slope of the cone in Fig. 3.

It can also be proved that the slope is inversely proportional to the amount of damage, thus implying that a higher crack density is favouring sliding.

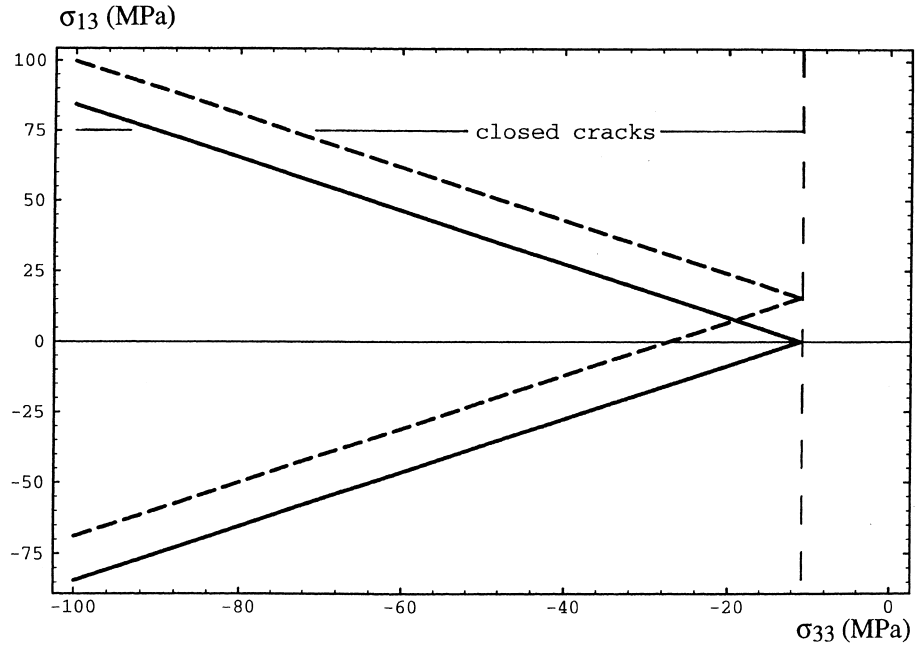

Fig. 3. Frictional sliding criterion and the relative sliding-induced hardening mechanism in the reduced stress-space ($\sigma_{33}-\sigma_{13}$) for $\boldsymbol{\gamma}^k=\mathbf{0}$ (solid line) and $\boldsymbol{\gamma}^k\neq\mathbf{0}$ (dashed line).

4. Damage and frictional sliding interaction: fully coupled model

The model completed in Section 3 incorporating friction-induced blocking and sliding on equivalent mesocrack-sets is valid for a given ('freezed') damage state or for conservative damage evolution ($\boldsymbol{D}^k$-proportional loading paths). It has proved conclusive in representing multistage loading and unloading dissipative cycles due to blocking and sliding sequences, see [13] for illustrations. In particular a dissipative unloading blocking and sliding sequence could be obtained while for the same stress–strain cycle the frictionless model of Section 2 gave purely elastic unloading, see Fig. 4 for a shear-loading cycle for pre-damaged material.

The splitting-like damage kinetics considered in Section 2 is approximately valid for closed sliding mesocracks even when some branching occurs see for example [25] for some experimental insight. This type of kinetics will be still considered as the predominant mechanism furthest for $\boldsymbol{D}^k$-non-proportional loading. This means the complementary damage law (7)–(8) being reconducted for more complex stress–strain paths involving varying $\boldsymbol{D}^k$ orientations. However, as the frictional blocking-and-sliding is inevitably affecting the stress–strain response, so for example the stress threshold corresponding to damage criterion $f=0$ is subsequently affected. For example in the stress subspace analogous to that of Fig. 3, the frontier $f=0$ corresponding to closed cracks under frictional blocking/sliding is farther beyond the limit for frictionless cracks, see e.g. Fig. 9 in [13].

This is mostly the sliding complementary rule (22)–(24) which needs to be perfected to describe fairly the $\boldsymbol{D}^k$-non-proportional loading paths. If the principal axes of $\boldsymbol{D}^k$ rotate the orthogonality $\boldsymbol{\gamma}^k$: $\boldsymbol{D}^k=0$ is no longer true and discontinuities may arise, especially for crack closure-opening transition. So, an enhanced form of $h^k\leqslant 0$ needs to account for the $\boldsymbol{D}^k$-axes rotation. The form (22), depending on $\boldsymbol{F}^{\gamma\mathrm{Tk}}$, produced – via normality rule (24) – sliding $\dot{\boldsymbol{\gamma}}^k$ *in* the mesocrack plane. A judicious modification of this basic assumption should be compatible with sliding and damage departure from the actual mesocrack equivalent plane. This is achieved by means of the following partition of $\boldsymbol{F}^{\gamma k}$, given below for a single crack set of normal $\boldsymbol{v}^k$:

$$\boldsymbol{F}^{\gamma k}=\boldsymbol{F}^{\gamma\mathrm{Tk}}+\boldsymbol{F}^{\gamma\mathrm{Nk}}=\underbrace{\boldsymbol{F}^{\gamma\mathrm{Tk}}+4\beta(\boldsymbol{\gamma}^k:\boldsymbol{D}^k)\,\boldsymbol{v}^k\otimes\boldsymbol{v}^k}-4\beta(\boldsymbol{\varepsilon}:\boldsymbol{D}^k)\,\boldsymbol{v}^k\otimes\boldsymbol{v}^k$$

$$=\qquad\boldsymbol{F}^k\qquad-4\beta(\boldsymbol{\varepsilon}:\boldsymbol{D}^k)\,\boldsymbol{v}^k\otimes\boldsymbol{v}^k. \tag{25}$$

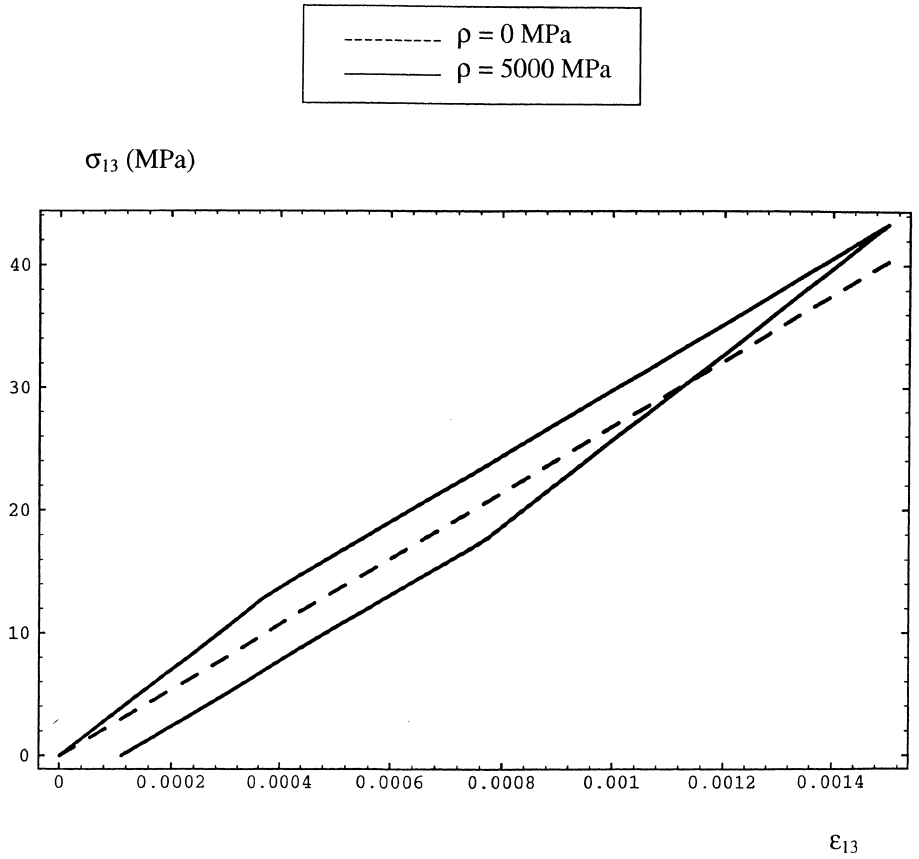

Fig. 4. Influence of friction coefficient on stress-strain response for a shear loading under constant damage (single crack system perpendicular to torsion axis).

$\boldsymbol{F}^k$ is the appropriate part of $\boldsymbol{F}^{\gamma k}$ to enter the more general expression of $h^k \leqslant 0$ suitable for the model including $\boldsymbol{D}^k$-axes rotation. First, one obtains that for $\boldsymbol{D}^k$-proportional loading $\boldsymbol{F}^k$ reduces to $\boldsymbol{F}^{\gamma \mathrm{Tk}}$(as $\boldsymbol{\gamma}^k$: $\boldsymbol{D}^k = 0$) and the new representation h^k ($\boldsymbol{F}^k$, $\boldsymbol{v}^k \cdot \boldsymbol{\varepsilon} \cdot \boldsymbol{v}^k$) reduces to (22). Secondly, the above-mentioned, crucial stress continuity problem is effectively dealt with. In fact, comparing (14), (21), (23), (26), one can see that the closure-opening transition point for sliding crack-set can be alternatively defined as:

$$\boldsymbol{F}^k = \boldsymbol{F}^{\gamma k} = \boldsymbol{0} \quad \Longleftrightarrow \quad \boldsymbol{\varepsilon} \cdot \boldsymbol{D}^k + \boldsymbol{D}^k \cdot \boldsymbol{\varepsilon} = \boldsymbol{\gamma}^k \cdot \boldsymbol{D}^k + \boldsymbol{D}^k \cdot \boldsymbol{\gamma}^k. \tag{26}$$

Despite the fact that the above equation represents weaker condition than (14), it allows to verify the singularity requirement for $[[\boldsymbol{C}^*]]$ (cf. Section 3.1) leading to the stress continuity.

It can be remarked that though $\boldsymbol{\gamma}^k : \boldsymbol{D}^k \neq 0$ as equivalent crack-axes rotate no additional invariants are necessary in the strain energy expression (18). They are not required by the continuity considerations (see above) and bring neither significant information. For example, introducing tr $\boldsymbol{\varepsilon}$ tr $(\boldsymbol{\gamma}^k \cdot \boldsymbol{D}^k)$, tr $\boldsymbol{\gamma}^k \cdot \mathrm{tr}(\boldsymbol{\gamma}^k \cdot \boldsymbol{D}^k)$ and $\boldsymbol{\gamma}^k$: D_k $\boldsymbol{L}^k$: $\boldsymbol{\gamma}^k$ contributes to no more record on shear moduli degradation than existing invariants $\mathrm{tr}(\boldsymbol{\varepsilon} \cdot \boldsymbol{\gamma}^k \cdot \boldsymbol{D}^k)$ and tr $(\boldsymbol{\gamma}^k \cdot \boldsymbol{\gamma}^k \cdot \boldsymbol{D}^k)$.

The above considerations lead to the following improved expression for the sliding complementary rule:

$$h^k(\boldsymbol{F}^k, \boldsymbol{v}^k \cdot \boldsymbol{\varepsilon} \cdot \boldsymbol{v}^k) = \sqrt{\frac{1}{2}\,\mathrm{tr}(\boldsymbol{F}^k \cdot \boldsymbol{F}^k)} + \rho \boldsymbol{v}^k \cdot \boldsymbol{\varepsilon} \cdot \boldsymbol{v}^k \leqslant 0, \tag{27}$$

$$\dot{\boldsymbol{\gamma}}^k = \Lambda_\gamma^k \frac{\partial h^k(\boldsymbol{F}^k, \boldsymbol{v}^k \cdot \boldsymbol{\varepsilon} \cdot \boldsymbol{v}^k)}{\partial \boldsymbol{F}^{\gamma k}} = \begin{cases} 0 & \text{if } \ h^k < 0 \quad \text{or} \quad h^k = 0, \dot{h}^k < 0, \\ \Lambda_\gamma^k \dfrac{\boldsymbol{F}^k}{\sqrt{2\mathrm{tr}(\boldsymbol{F}^k \cdot \boldsymbol{F}^k)}} & \text{if } \ h^k = 0 \quad \text{and} \quad \dot{h}^k = 0, \Lambda_\gamma^k \geqslant 0. \end{cases} \tag{28}$$

The direction of $\dot{\boldsymbol{\gamma}}^k$ is thus allowed to leave the equivalent crack-set plane consecutively to the rotation of the latter. In such a manner $\boldsymbol{D}^k$-non-proportional loading can be followed by the model which takes into account the interaction of the two dissipative mechanisms : damage and frictional sliding. The corresponding combined dissipation is:

$$D = \boldsymbol{F}^{\mathrm{D}} : \dot{\boldsymbol{D}} + \sum_{k=1}^{3} \boldsymbol{F}^{\gamma k} : \dot{\boldsymbol{\gamma}}^k. \tag{29}$$

Despite of the corresponding normality rules, i.e. the formulae (8) and (29), respectively for damage growth and frictional sliding, and the convexity characterizing the domains $f \leqslant 0$ and $h \leqslant 0$ one should check the non-negativity of D in the process of numerical integration. This is because of the partition of the respective thermodynamic forces, i.e. the sole parts $\boldsymbol{F}^D - \boldsymbol{F}^{D2} - \boldsymbol{F}^{D1}$ and $\boldsymbol{F}^{\gamma k} - [-4\beta\ (\boldsymbol{\varepsilon} : \boldsymbol{D}^k)\ \boldsymbol{v}^k \otimes \boldsymbol{v}^k]$ entering, respectively into the corresponding damage and sliding-yield functions. The convex domains at stake should contain their origin, respectively in the $\boldsymbol{F}^D$-space and in $\boldsymbol{F}^{\gamma k}$-space to ensure thermodynamically admissible evolutions (one can note in this point some analogy with the kinematic hardening rule in classical plasticity). In this respect the algorithmic approximation of the coupled model should control the dissipation issue for each step and integration point. The incremental procedure leading to numerical integration of the equations of the model is summarized Section 5.

For completeness, the coupled rate-independent anisotropic damage-frictional sliding constitutive equations are summarized in Table 1.

Table 1
Rate-independent anisotropic damage-friction coupled model

Free energy: (per unit volume)	$w(\boldsymbol{\varepsilon}; \boldsymbol{D}, \boldsymbol{\gamma}) = \frac{1}{2}\lambda\ (\mathrm{tr}\ \boldsymbol{\varepsilon})^2 + \mu\ \mathrm{tr}\ (\boldsymbol{\varepsilon}\cdot\boldsymbol{\varepsilon}) + g\ \mathrm{tr}\ (\boldsymbol{\varepsilon}\cdot\boldsymbol{D}) + \alpha\ \mathrm{tr}\ \boldsymbol{\varepsilon}\ \mathrm{tr}\ (\boldsymbol{\varepsilon}\cdot\boldsymbol{D}) + 2\beta\ \mathrm{tr}\ (\boldsymbol{\varepsilon}\cdot\boldsymbol{\varepsilon}\cdot\boldsymbol{D}) + \sum_{k=1}^{3} H(-\boldsymbol{v}^k\cdot\boldsymbol{\varepsilon}\cdot\boldsymbol{v}^k)\big[-\alpha\boldsymbol{\varepsilon} : (D_k\boldsymbol{L}^k) : \boldsymbol{\varepsilon} - 2\beta\ \mathrm{tr}\ (\boldsymbol{\varepsilon}\cdot\boldsymbol{\varepsilon}\cdot\boldsymbol{D}^k) + 4\beta\ \mathrm{tr}\ (\boldsymbol{\varepsilon}\cdot\boldsymbol{\gamma}^k\cdot\boldsymbol{D}^k) - 2\beta\ \mathrm{tr}\ (\boldsymbol{\gamma}^k\cdot\boldsymbol{\gamma}^k\cdot\boldsymbol{D}^k)\big].$
Stress–strain and internal variable relations:	$\boldsymbol{\sigma} = \frac{\partial w}{\partial \boldsymbol{\varepsilon}},$ see (19) $\boldsymbol{F}_D = -\frac{\partial w}{\partial \boldsymbol{D}},$ see (20); $\boldsymbol{F}^{\gamma k} = -\frac{\partial w}{\partial \boldsymbol{\gamma}^k},$ see (21) for details
Damage complementary rule:	$f(\boldsymbol{F}^D - \boldsymbol{F}^{D2} - \boldsymbol{F}^{D1-}, \boldsymbol{D}) \leqslant 0,$ see (7) for details $\dot{\boldsymbol{D}} = \Lambda_D \frac{\partial f}{\partial \boldsymbol{F}^D} = \Lambda_D \left[\frac{\boldsymbol{\varepsilon}^+}{\sqrt{2\ \mathrm{tr}(\boldsymbol{\varepsilon}^+\cdot\boldsymbol{\varepsilon}^+)}} + B\,\boldsymbol{D}\right],\ \Lambda_D \geqslant 0.$
$\boldsymbol{D}$-consistency:	$\dot{f}\Lambda_D = 0.$
Frictional sliding related plasticity:	$h^k(\boldsymbol{F}^k, \boldsymbol{v}^k\cdot\boldsymbol{\varepsilon}\cdot\boldsymbol{v}^k) = \sqrt{\frac{1}{2}\ \mathrm{tr}\ (\boldsymbol{F}^k\cdot\boldsymbol{F}^k)} + \rho\ \boldsymbol{v}^k\cdot\boldsymbol{\varepsilon}\cdot\boldsymbol{v}^k \leqslant 0,$ see (23), (25) for detailed form of $\boldsymbol{F}^k$
	$\dot{\boldsymbol{\gamma}}^k = \Lambda_\gamma^k \frac{\partial \mathrm{h}^k}{\partial\ \boldsymbol{F}^{\gamma k}} = \Lambda_\gamma^k \frac{\boldsymbol{F}^k}{\sqrt{2\mathrm{tr}\ (\boldsymbol{F}^k\cdot\boldsymbol{F}^k)}} \quad \Lambda_\gamma^k \geqslant 0$
$\boldsymbol{\gamma}^k$-consistency:	$\dot{h}^k\Lambda_\gamma^k = 0$

5. Numerical implementation; identification of material constants; applications: rock-like solids

5.1. Integration of damage and sliding constitutive relations

This subsection provides an outline of several computational aspects involved in the finite-element implementation of the model presented above. The incremental weak form of the equilibrium equation is formulated for a body $\boldsymbol{\Omega} \subset R^3$ with boundary $\partial\boldsymbol{\Omega}$ in the time interval $t \in I = [O, T]$. Let $\boldsymbol{f}_d$ be the given body forces per unit volume, $\boldsymbol{u}_d$ the displacements imposed on the part $\partial_1\boldsymbol{\Omega}$ of $\partial\boldsymbol{\Omega}$ and $\boldsymbol{F}_d$ the traction vectors prescribed on the complementary part $\partial_2\boldsymbol{\Omega}$. With the time partition : $I = U_{r=1}^{N}[t_r, t_{r+1}]$, the weak problem is formulated as follows: for each time increment $[t_r, t_{r+1}]$, find the displacement field $\boldsymbol{u}$ such as, at time t_{r+1},

$$\int_{\boldsymbol{\Omega}} \boldsymbol{\sigma}(\nabla_s \boldsymbol{u}) : \nabla_s \boldsymbol{\delta u} \, \mathrm{d}\boldsymbol{\Omega} - \int_{\boldsymbol{\Omega}} \boldsymbol{f}_d(t_{r+1}) \cdot \boldsymbol{\delta u} \, \mathrm{d}\boldsymbol{\Omega} - \int_{\partial_2\boldsymbol{\Omega}} \boldsymbol{F}_d(t_{r+1}) \cdot \boldsymbol{\delta u} \, \mathrm{d}S = 0 \tag{30}$$

with $\boldsymbol{u} \in U_{ad}, U_{ad} = \{\boldsymbol{u} | \boldsymbol{u} = \boldsymbol{u}_d(t_{r+1}) \text{ on } \partial_1\boldsymbol{\Omega}\}$ and $\forall \delta\boldsymbol{u} \in U_0, U_0 = \{\boldsymbol{u} | \boldsymbol{u} = \boldsymbol{0} \text{ on } \partial_1\boldsymbol{\Omega}\}$.

The highly non-linear character of the constitutive laws, brought together in Sections 2–4, requires that a time integration algorithm for the evolution of the damage variable $\boldsymbol{D}$ and of the sliding variable $\boldsymbol{\gamma}$ be accurate and stable. Such an algorithm forms, together with a spatial finite-element discretization, the finite-element implementation of the problem outlined above.

The incremental procedure leading to numerical integration of the equations of the model consists in the standard strain discretization for the loading path under consideration. At time t_r the strain $\boldsymbol{\varepsilon}_r$, the internal variables $\boldsymbol{D}_r$ and $\boldsymbol{\gamma}_r^k$ as well as the stress $\boldsymbol{\sigma}_r$ are known. The stress $\boldsymbol{\sigma}_{r+1}$ and the internal variables $\boldsymbol{D}_{r+1}$ and $\boldsymbol{\gamma}_{r+1}^k$ at time t_{r+1} are looked for. Since each dissipative mechanism (damage and sliding) may occur independently and since each of them offers some particularities, the two corresponding integration algorithms are commented separately. The coupling is discussed afterwards.

(i) Local integration for the damage model.

The damage evolution Eq. (8) is integrated point-wise (at each quadrature point of a finite-element in the spatial discretization) in the strain-driven setting. The set of state variables $\boldsymbol{q}_r$ are assumed to be known at the end of the step $r : \boldsymbol{q}_r = (\boldsymbol{\varepsilon}_r, \boldsymbol{D}_r, \boldsymbol{\gamma}_r^k)$. Since only damage evolution is concerned in this paragraph, $\boldsymbol{\gamma}^k$ is considered constant, i.e. $\boldsymbol{\gamma}_{r+1}^k = \boldsymbol{\gamma}_r^k$. The integration problem amounts to updating the mechanical state, i.e. to determine $\boldsymbol{q}_{r+1}$ and $\boldsymbol{\sigma}_{r+1}$, from $\boldsymbol{q}_r$ and prescribed strain increment $\Delta\boldsymbol{\varepsilon}$ (such as $\boldsymbol{\varepsilon}_{r+1} = \boldsymbol{\varepsilon}_r + \Delta\boldsymbol{\varepsilon}$):

$$\begin{aligned} &\boldsymbol{q}_{r+1} = \left(\boldsymbol{\varepsilon}_{r+1}, \boldsymbol{D}_{r+1}, \boldsymbol{\gamma}_{r+1}^k\right) \quad \text{with} \quad \boldsymbol{\varepsilon}_{r+1} = \boldsymbol{\varepsilon}_r + \Delta\boldsymbol{\varepsilon}, \boldsymbol{D}_{r+1} = \boldsymbol{D}_r + \Delta\boldsymbol{D} \\ &\boldsymbol{\sigma}_{r+1} = \boldsymbol{G}_\sigma \left(\boldsymbol{\varepsilon}_{r+1}, \boldsymbol{D}_{r+1}, \boldsymbol{\gamma}_{r+1}^k\right), \end{aligned} \tag{31}$$

where the symbol $\mathbf{G}_\sigma$ summarizes Relation (19).

The following scheme furnishes a well-grounded, stable algorithm for the damage model:

(a) Calculation of the components of $\boldsymbol{\varepsilon}_{r+1}^+$:

Given $\boldsymbol{\varepsilon}_{r+1}$, $\boldsymbol{Q}_{r+1}^+$ and then $\boldsymbol{P}_{r+1}^+$ are directly determined from the expression $P_{ijkl}^+ = Q_{ik}^+ Q_{jl}^+$, where $\boldsymbol{Q}^+ = \sum_{n=1}^{3} H(\boldsymbol{\varepsilon}_n) \boldsymbol{q}^n \otimes \boldsymbol{q}^n$; $\boldsymbol{\varepsilon}_n$, $\boldsymbol{q}^n$ being the eigenvalues and eigenvectors of $\boldsymbol{\varepsilon}$, H the Heaviside function. $\boldsymbol{P}_{r+1}^+$ extracts the positive components of $\boldsymbol{\varepsilon}_{r+1}$:

$$\boldsymbol{\varepsilon}_{r+1}^+ = \boldsymbol{P}_{r+1}^+ : \boldsymbol{\varepsilon}_{r+1}.$$

(b) Elastic predictor:

The increment is first assumed to be purely elastic:

$$\Delta\boldsymbol{D} = \boldsymbol{0}, \quad \boldsymbol{D}_{r+1} = \boldsymbol{D}_r.$$

The value of $f(\boldsymbol{\varepsilon}_{r+1}, \boldsymbol{D}_r)$ is then checked:

$$f(\boldsymbol{\varepsilon}_{r+1}, \boldsymbol{D}_r) = \sqrt{\frac{g^2}{2}\ \mathrm{tr}(\boldsymbol{\varepsilon}^+_{r+1} \cdot \boldsymbol{\varepsilon}^+_{r+1})} - Bg\ \mathrm{tr}(\boldsymbol{\varepsilon}^+_{r+1} \cdot \boldsymbol{D}_r) - (C_0 + C_1\ \mathrm{tr}\ \boldsymbol{D}_r). \tag{32}$$

If $f(\boldsymbol{\varepsilon}_{r+1},\ \boldsymbol{D}_r) \leqslant 0$, the elastic prediction is confirmed and $\boldsymbol{q}_{r+1}$ is updated with $\boldsymbol{D}_{r+1} = \boldsymbol{D}_r$. Otherwise, $\boldsymbol{D}_{r+1}$ has to be corrected and $\Delta\boldsymbol{D}$ is calculated as follows.

(c) Damage correction:

The damage increment is given by the evolution equation (8) in its discretized form:

$$\Delta\boldsymbol{D} = \Delta\boldsymbol{\Lambda}_D \left[\frac{\boldsymbol{\varepsilon}^+_{r+\theta}}{\sqrt{2\mathrm{tr}(\boldsymbol{\varepsilon}^+_{r+\theta} \cdot \boldsymbol{\varepsilon}^+_{r+\theta})}} + B\boldsymbol{D}_{r+\theta} \right], \tag{33}$$

where one writes:

$$\boldsymbol{\varepsilon}^+_{r+\theta} = (1-\theta)\ \boldsymbol{\varepsilon}^+_r + \theta\ \boldsymbol{\varepsilon}^+_{r+1},$$

$$\boldsymbol{D}_{r+\theta} = (1-\theta)\ \boldsymbol{D}_r + \theta\ \boldsymbol{D}_{r+1}.$$

The choice of $\theta = 1$ corresponds to a purely implicit integration scheme ; in this framework, Cormery [26] showed that the damage condition $f(\boldsymbol{\varepsilon}_{r+\theta}, \boldsymbol{D}_{r+\theta}) = 0$ with $\theta = 1$ reduces to a simple linear equation in $\Delta\boldsymbol{\Lambda}_D$. The solution of this equation is:

$$\Delta\boldsymbol{\Lambda}_D = \frac{A_{r+1}}{B\,A_{r+1} + C_1 C_{r+1} + Bg\mathscr{F}_{r+1}} \tag{34}$$

with

$$A_{r+1} = \sqrt{\frac{g^2}{2}\ \mathrm{tr}(\boldsymbol{\varepsilon}^+_{r+1} \cdot \boldsymbol{\varepsilon}^+_{r+1})} - B\ g\ \mathrm{tr}(\boldsymbol{\varepsilon}^+_{r+1} \cdot \boldsymbol{D}_r) - (C_0 + C_1\ \mathrm{tr}\ \boldsymbol{D}_r)$$

$$C_{r+1} = \frac{\mathrm{tr}\ \boldsymbol{\varepsilon}^+_{r+1}}{\sqrt{2\ \mathrm{tr}(\boldsymbol{\varepsilon}^+_{r+1} \cdot \boldsymbol{\varepsilon}^+_{r+1})}} + B\ \mathrm{tr}\ \boldsymbol{D}_r$$

$$\mathscr{F}_{r+1} = \sqrt{\frac{1}{2}\mathrm{tr}(\boldsymbol{\varepsilon}^+_{r+1} \cdot \boldsymbol{\varepsilon}^+_{r+1})} + B\ \mathrm{tr}(\boldsymbol{\varepsilon}^+_{r+1} \cdot \boldsymbol{D}_r)$$

$\Delta\boldsymbol{D}$ is then known as well as the mechanical state $\boldsymbol{q}_{r+1}$.

Remarks: A purely implicit integration scheme has been chosen. Indeed, Ortiz and Popov [27] showed for a general formulation of elastoplasticity that this scheme ensures unconditionnally stability properties of relevant integration algorithms, whatever the strain increment $\Delta\boldsymbol{\varepsilon}$ is, even for strongly non-linear behaviour. Moreover, this scheme is well adapted to the above damage model : the value of $\Delta\boldsymbol{\Lambda}_{\mathrm{D}}$ is the solution of a linear equation enforcing incremental damage consistency condition and does not require iterative procedure, unlike for most of elastoplastic models.

(ii) Local integration for the sliding model.

Damage is tentatively assumed to be constant ($\boldsymbol{D}_{r+1} = \boldsymbol{D}_r$). The key aspect in the formulation of the discrete time stepping procedure for the frictional sliding related plasticity concerns the integration of (24) or (28) for general, damage axes rotation accompanied loading), the evolution equation for the sliding variable $\boldsymbol{\gamma}^k$. The elastic predictor/plastic corrector scheme is employed here in a way parallel to damage integration.

(a) Elastic predictor:

One assumes $\Delta\boldsymbol{\gamma}^k = \boldsymbol{0}$ (i.e. $\boldsymbol{\gamma}^k_{r+1} = \boldsymbol{\gamma}^k_r$). The damage eigenvalues D^k_{r+1} and eigenvectors $\boldsymbol{v}^k_{r+1}$ are known, the part $\boldsymbol{F}^k_{r+1}$ of the thermodynamic force related to $\boldsymbol{\gamma}^k$ entering the expression of h^k is given by (see (25)):

$$\boldsymbol{F}^k_{r+1} = \boldsymbol{F}^{\gamma k}_{r+1} + 4\beta\ D^k_{r+1}(\boldsymbol{v}^k_{r+1} \cdot \boldsymbol{\varepsilon}_{r+1} \cdot \boldsymbol{v}^k_{r+1})\ \boldsymbol{v}^k_{r+1} \otimes \boldsymbol{v}^k_{r+1}. \tag{35}$$

The value of h^k is checked:

$$h^k(\boldsymbol{F}^k_{r+1}, \boldsymbol{v}^k_{r+1}\cdot\boldsymbol{\varepsilon}_{r+1}\cdot\boldsymbol{v}^k_{r+1}) = \sqrt{\frac{1}{2}\,\mathrm{tr}(\boldsymbol{F}^k_{r+1}\cdot\boldsymbol{F}^k_{r+1})} + \rho\,\boldsymbol{v}^k_{r+1}\cdot\boldsymbol{\varepsilon}_{r+1}\cdot\boldsymbol{v}^k_{r+1}. \tag{36}$$

If $h^k \cdot 0$, the set of variables $\boldsymbol{q}_{r+1} = (\boldsymbol{\varepsilon}_{r+1}, \boldsymbol{D}_{r+1}, \boldsymbol{\gamma}^k_{r+1})$ as well as $\boldsymbol{\sigma}_{r+1}$ is then determined as confined to reversible domain. If $h^k > 0$, the mechanical state has to be corrected, i.e. frictional sliding evolution accounted for through the plastic correction below.

(b) Plastic correction:

The aim is to solve the following system:

$$\boldsymbol{\sigma}_{r+1} = \boldsymbol{G}_\sigma(\boldsymbol{\varepsilon}_{r+1}, \boldsymbol{D}_{r+1}, \boldsymbol{\gamma}^k_{r+1}), \tag{37a}$$

$$\boldsymbol{F}^{\gamma k}_{r+1} = \boldsymbol{G}_{F\gamma k}(\boldsymbol{\varepsilon}_{r+1}, \boldsymbol{\gamma}^k_{r+1}), \tag{37b}$$

$$\Delta\boldsymbol{\gamma}^k = \Delta\boldsymbol{\Lambda}^k_\gamma \boldsymbol{G}_\gamma(\boldsymbol{F}^k_{r+\theta}), \tag{37c}$$

$$h^k_{r+1} = 0, \tag{37d}$$

where (37a)–(37c), respectively stand for Eqs. (19), (21) and (24).

Unlike the case of damage integration, the implicit scheme applied to sliding does not lead to the resolution of a linear equation for $\Delta\boldsymbol{\Lambda}^k_\gamma$: (37a)–(37d) is a set of non-linear algebraic equations to be solved for the unknowns $\boldsymbol{\sigma}_{r+1}$, $\boldsymbol{\gamma}^k_{r+1}$, $\boldsymbol{F}^{\gamma k}_{r+1}$ and $\Delta\boldsymbol{\Lambda}^k_\gamma$. The solution is approximated by a Newton–Raphson algorithm.

(iii) Coupling

Both above dissipative mechanisms (damage and frictional sliding) may occur along particular loading paths. The problem is then to determine the increments $\Delta\boldsymbol{D}$ and $\Delta\boldsymbol{\gamma}^k$ simultaneously. The integration is here facilitated by the low degree of coupling between f on one hand and h^k on the other : whereas h^k is a function of $\boldsymbol{D}$ and $\boldsymbol{\gamma}^k$, f depends only on $\boldsymbol{D}$ and Eq. (33) can be solved without explicit reference to sliding. The general algorithm is as follows:

(1) The value $\boldsymbol{v}^k\cdot\boldsymbol{\varepsilon}\cdot\boldsymbol{v}^k$ of the normal strain for each equivalent microcrack system is checked.

(2) If $\boldsymbol{v}^k\cdot\boldsymbol{\varepsilon}\cdot\boldsymbol{v}^k > 0$, the corresponding system is open ; sliding does not occur and $\Delta\boldsymbol{D}$ is calculated as described in paragraph (i).

(3) If $\boldsymbol{v}^k\cdot\boldsymbol{\varepsilon}\cdot\boldsymbol{v}^k \leqslant 0$, the corresponding system is closed and may slide. Both criteria $f \leqslant 0$, $h^k \leqslant 0$ are checked; $\Delta\boldsymbol{D}$ and $\Delta\gamma^k$ are calculated by solving successively Eqs. (33) and (37c). The relation (37a) generalized to coupled process yields $\boldsymbol{\sigma}_{r+1}$.

5.2. Identification of the material parameters

The model presented in Sections 2–4 has been conceived for engineering applications. The emphasis has been put on the accessibility of a small number of material constants : only nine parameters are required for fully coupled model (λ, μ, α, β, g, C_0, C_1, B, ρ). Seven of them can be relatively easily determined by conventional axisymmetric "triaxial" compression tests (Fig. 5). The friction coefficient ρ is identified by torsional tests involving frictional sliding. To determine B, a less common off-axis loading for pre-damaged specimen has to be exploited. The identification procedure has been described in details by Pham [28] and Cormery [26]. Some guiding indications are summarized below.

Consider a triaxial compression test on a cylindrical sample assumed as approximately initially undamaged and isotropic. One can determine the conventional elastic constants λ and μ from E_o and ν_o (initial Young modulus and Poisson ratio) relevant to the stress–strain relationships $(\sigma_3 - \sigma_1)$ vs. ε_3 and $(\sigma_3 - \sigma_1)$ vs. ε_1, respectively, in the elastic range without damage growth ($f < 0$). To determine the values of α, β and g, the non-linear, i.e. damage affected portion and the subsequent unloading are exploited. The point at which unloading is performed should correspond to pronounced oriented damage but has to be reasonably far from the localization bifurcation-onset point to avoid interference. The unloading portion corresponding to $\boldsymbol{D}$-modified degraded moduli is being linearized according to the frictionless damage-elastic model (Section 2). By inverting (5) and specifying to axisymmetric stress–strain-damage path one can

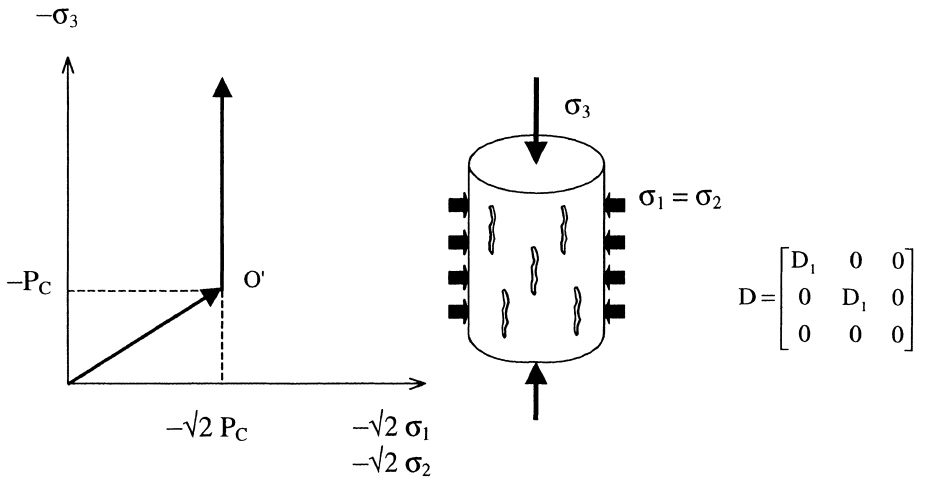

Fig. 5. Conventional triaxial compression loading path.

establish finally three independent equations (Eqs. (38)–(40) below) with respect to the unknowns αD_1, βD_1 and gD_1.

Let be B and B' the starting point for the unloading (see Fig. 6). The values of αD_1 and βD_1 are related to E_3 and v_{31} (i.e. the unloading slopes) by:

$$E_3 = \lambda + 2\mu - \frac{L_2^2}{L_1}, \tag{38}$$

$$v_{31} = \frac{L_2}{2L_1} \tag{39}$$

with

$$L_1 = \lambda + \mu + 2(\alpha + \beta)D_1 \quad L_2 = \lambda + \alpha D_1.$$

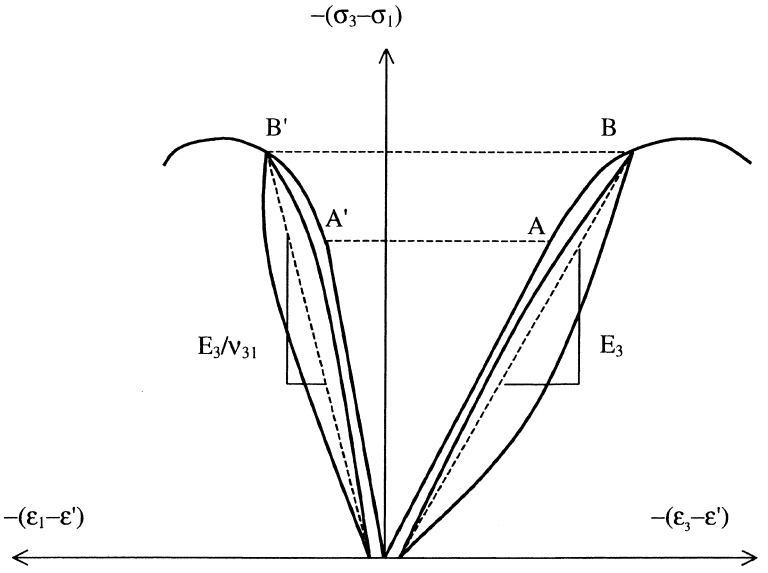

Fig. 6. Determination of degraded elastic moduli.

The expression related to damage-induced residual effects can be expressed as follows:

$$gD_1 = \frac{E_3\varepsilon_3 - \sigma_3 + 2\nu_{31}\sigma_1}{2\nu_{31}}. \tag{40}$$

The next stage consists in determining C_0 and C_1. At the initial damage threshold on the experimental curves (points A and A'), we have from (7):

$$|g|\varepsilon_1^A - C_0 = 0. \tag{41}$$

At the above-mentioned unloading point B, damage has reached a given value D_1; checking the criterion leads to:

$$|g|\varepsilon_1^B - (C_0 + 2\,C_1\,D_1) = 0. \tag{42}$$

According to the actual 'phenomenological' procedure based solely on stress–strain curves, one needs now to 'disentangle' the expressions αD_1, βD_1, gD_1, C_1D_1, i.e. find D_1 corresponding to the loading–unloading point B in order to obtain the constants involved. This is the purpose of the final stage of the identification at stake and is done by an iterative procedure comprising the following steps:

(i) set any admissible value D_1 as (tentative) damage at the point concerned and calculate α, β, g, C_1 and C_0 from Eqs. (38)–(42);

(ii) calculate $-(\sigma_3 - \sigma_1)$ vs. ε_1 and ε_3, respectively;

(iii) check locally and/or globally the gap between the trial values (ii) and the experimental ones with a norm set in advance;

(iv) if no convergence, loop backwards to (i) with a new D_1. The choice of a loading–unloading point can eventually be reviewed.

The set (λ, μ, α, β, g, C_0, C_1) may thus be formally determined by means of a single loading–unloading test in axisymmetric triaxial apparatus. In fact it is preferable to cover a reasonable range of confining pressure values, i.e. exploit several curves and settle ultimate values of the constants concerned through averaging process. The hypothesis of an initially 'virgin' undamaged and isotropic solid can be eventually circumvented and an initial microcrack-damage state may be accounted for. Some initial, non-damage-induced anisotropy may be eventually introduced as f.ex. for ceramic–matrix composites. However, it requires additional terms in the energy representation, see [29].

To determine ρ for friction-induced plasticity, one resorts to torsional tests: on experimental curves giving the torque C vs. the angular deformation w (see Fig. 9 at the end of this section), the first loss of linearity is due to the onset of frictional sliding. For this point, the sliding yield condition is reached and solving $h^k = 0$ provides the value of ρ.

A partial identification, discarding the constant B set to zero has been performed for a Vosges sandstone tested by Pecqueur [20] (Table 2) and a Fontainebleau sandstone (Table 3).

Table 2
Constitutive parameters (Vosges sandstone)

λ (MPa)	μ (MPa)	α (MPa)	β (MPa)	g (MPa)	C_0 (MPa)	C_1 (MPa)	B	ρ (MPa)
3250	4875	9925	−11180	−32	0.02	0.27	0	1565

Table 3
Constitutive parameters (Fontainebleau sandstone)

λ (MPa)	μ (MPa)	α (MPa)	β (MPa)	g (MPa)	C_0 (MPa)	C_1 (MPa)	B	ρ (MPa)
26 250	17 500	1900	−20 400	−110	0.001	0.55	0	2500

5.3. Applications: rock-like solids

To illustrate the pertinency of the coupled model and efficiency of the integration algorithms summarized above two selected numerical examples are given below. They are concerned with brittle rock behaviour and examine the effect of loading involving necessarily the closed mesocrack related phenomena thus bringing forward the efficiency of the fully coupled model.

The first example is the analysis of a homogeneous stress–strain path relative to the third step of the complex loading programme as follows (see Fig. 7):

- Step a: Uniaxial tension, $\sigma_3 > 0$, induces damage $D_3 > 0$ (a set of parallel mesocracks of normal 3).
- Step b: Unloading then reloading under compression beyond the crack closure threshold are considered. The corresponding numerical simulation is strain-controlled; $\varepsilon_{33} < \varepsilon_{11} = \varepsilon_{22}$.
- Step c: Upon a given (freezed) configuration (ε_{33}, $\varepsilon_{11} = \varepsilon_{22}$) corresponding to mesocracks closure is superposed additional shear strain-controlled loading: $\varepsilon_{13} = \varepsilon_{23}$ and subsequent unloading. Three loading–unloading cycles are simulated. In Fig. 8 the corresponding σ_{13} vs. ε_{13} loading and unloading curves are

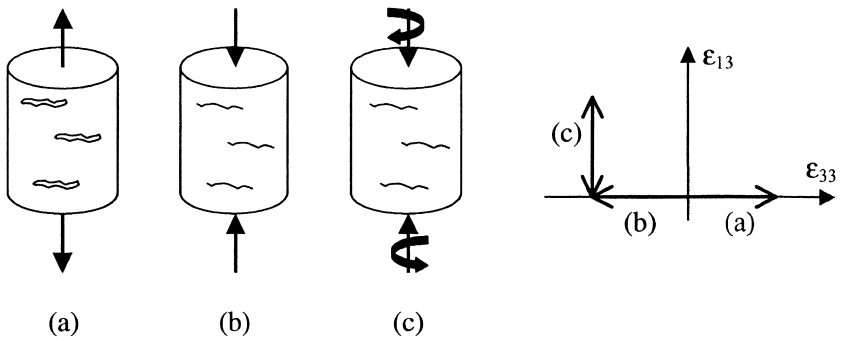

Fig. 7. Steps of the homogeneous torsion-and-compression simulation (the corresponding cyclic stress–strain curve is shown in Fig. 8).

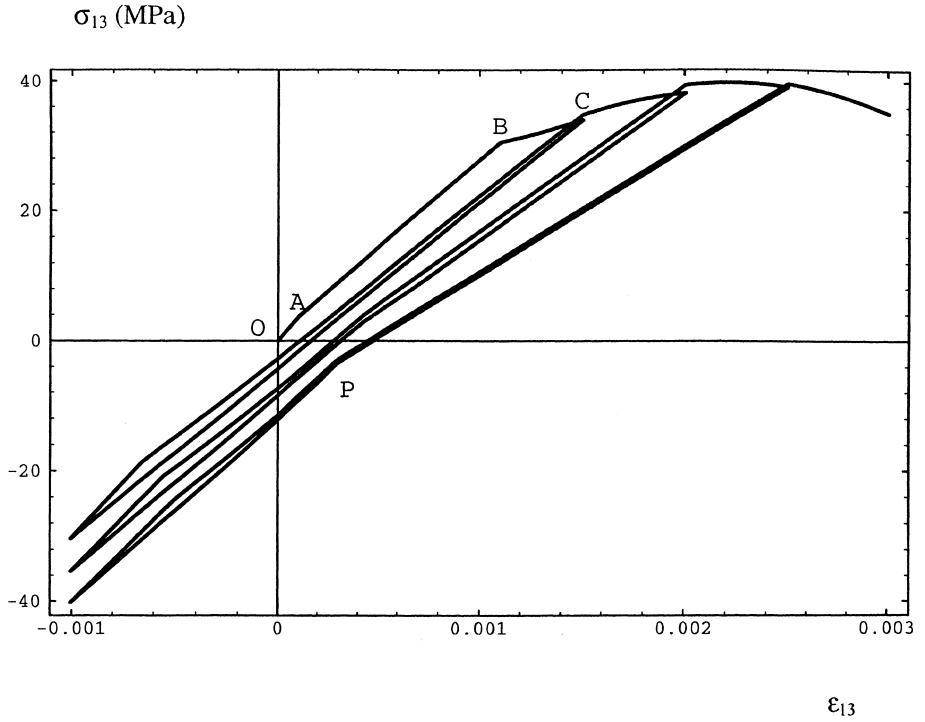

Fig. 8. Shear stress σ_{13}-shear strain ε_{13} loading and unloading cycles corresponding to damage and frictional sliding variation. Non-propotional damage growth is simulated preceded by an initial tension-induced damage ($D_3 > 0$) and subsequent compression-induced crack closure. Complex hysteresis is exhibited.

plotted. Damage growth, accompanied with principal ***D***-axes rotation is calculated for each loading cycle. Friction blocking or sliding effects are accounted for.

The initial stiffened portion O–A in Fig. 8 is due to friction-induced blocking effect corresponding to recovery of the solid elastic shear modulus μ. Beyond A frictional sliding is evolving, the slope of the portion A–B is lower than the slope 0–A. From B to C damage growth accompanied with frictional sliding occurs. The loading path at stake is a ***D***-non-proportional one; there is some rotation of equivalent crack-axes and a complex damage state is brought about. The unloading portions are here non-linear curves: multiform unloading process with successive sliding sequences occur (blocking on one equivalent set, two remaining sets open, followed by closure of a second one and frictional sliding on one then two sets, etc). Here, the simulated curve σ_{13} vs. ε_{13} is presented to illustrate the capacity of the model to deal with multiple stage loading/unloading loops involving eventually coupled damage-and-sliding effects and stiffening due to crack closure (for example, at point P, for the last unloading). The material under consideration is Fontainebleau sandstone (Table 3).

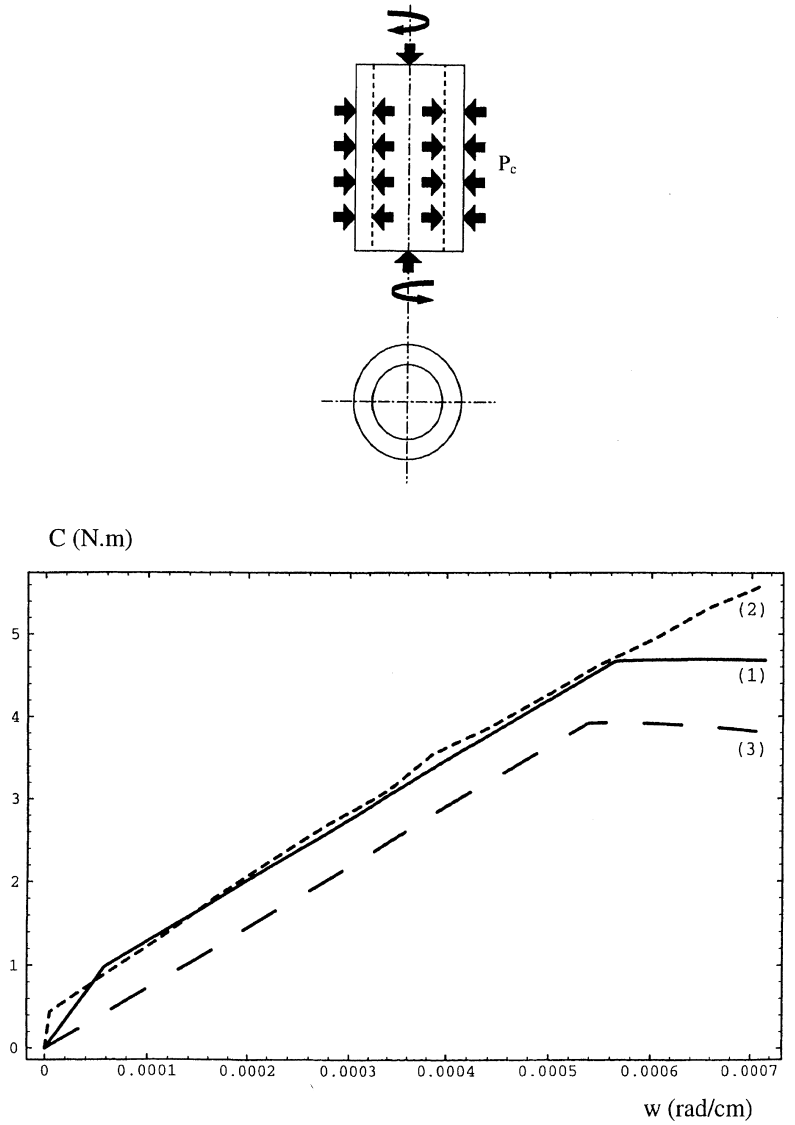

Fig. 9. Torque C vs. angular deformation w for hollow cylinder example. The solid line (1) gives homogeneous response (for $P_c = 10$ MPa) of the model when both damage and frictional blocking/sliding (for closed mesocracks) are active. It appears fairly close to experimental response (dashed line (2)). The frictionless model response is given by the dashed line (3).

The second example refers to experimental tests by Pecqueur et al. [19], Pecqueur [20], consisting in a torsional loading applied to hollow cylinder specimens under hydrostatic compression. The cylinder is cut in brittle rock (Vosges sandstone, Table 2). Pecqueur [20] showed that the stress field is homogeneous in the central third of the cylinder. Based on this statement, the following homogeneous simulation has been carried out : an hydrostatic compression ($P_c = 10$ MPa) is first applied to a pre-damaged material with a set of mesocracks perpendicular to the cylinder axis in compression-induced closure range, next a torque C is superimposed.

Again, an initial stiffened portion is observed corresponding to friction-related blocking phenomenon. It is followed by a stage where frictional sliding evolution is noticed. This explains the reduced slope observed in Fig. 9, the solid line (1) leaning closely to the experimental dashed one (2). Finally, for the last stage, the simultaneous complex damage growth and sliding take place and the slope becomes even smaller. The same simulation (with the same initial damage level and configuration) has been carried out for a prior version of the model (dashed line (3)) involving only the anisotropic damage propagation (cracks are allowed to slide, but without friction (Dragon et al. [11])). The curves clearly indicate that the hypothesis of perfectly lubricated cracks underestimates the torque value whereas friction stiffens the material and predicts a behaviour closer to experiment.

6. Conclusion

Two dissipative mechanisms, namely damage by microcracking and frictional sliding over internal crack surfaces, are considered in the framework of the three-dimensional model presented, applicable for quasi-brittle rock-like solids. The internal variable formalism employed for the joint process under consideration is based on second-order tensorial representation of damage and sliding effects respectively. The critical issue of the control of microcrack closure and opening phenomena is dealt with in the spirit of continuum damage approach associated with rigorous analysis of the stiffness recovery for closed microcracks. The basic simplifying assumption, carried on through the proposed modelling, consists in contraction of any real microcrack-set configuration (containing a number of sets) to an equivalent configuration of three mutually orthogonal systems. The analysis has been restricted furthermore to non-interacting crack systems regarding the energy expression even if the microcrack related damage evolution depends on current damage form.

The model constitutes an attempt to construct a tool applicable for efficient structural analysis through its relatively easy identifiability and algorithmic feasibility. In the same time a strong micromechanical motivation is being preserved in corresponding developments. It can be situated as an intermediary modelling approach between genuine micromechanical studies and pure phenomenological ones.

The examples presented illustrating joint damage and frictional sliding induced non-linear stress–strain behaviour reproduce remarkable non-linear effects of quasi-brittle (pseudo-plastic) solids like volumetric dilatancy, induced anisotropy and a characteristic multistage hysteresis in loading–unloading-reloading cycles. Some potentiality concerning fatigue description emerges from the analysis and results presented. The prospective study of transition from non-linear degradation towards local failure through localization bifurcation study in the presence of *joint* damage and frictional sliding evolution may allow to forge ahead towards a complete progressive degradation-failure incipience theory for quasi-brittle materials.

References

[1] V.A. Lubarda, D. Krajcinovic, Some fundamental issues in rate theory of damage-elastoplasticity, Int. J. Plasticity 11 (1995) 763–797.
[2] J.B. Walsh, The effect of cracks on the uniaxial elastic compression of rocks, J. Geophys. Res. 70 (1965) 399–411.
[3] M. Kachanov, A microcrack model of rock inelasticity–part I: frictional sliding on microcracks, Mech. Mater. 1 (1982) 19–27.
[4] H. Horii, S. Nemat-Nasser, Overall moduli of solids with microcracks: load-induced anisotropy, J. Mech. Phys. Solids 31 (1983) 151–171.
[5] J.W. Ju, On two-dimensional self-consistent micromechanical damage models for brittle solids, Int. J. Solids Struct. 27 (1991) 227–258.

[6] D. Krajcinovic, M. Basista, D. Sumarac, Basic principles, in: R. Talreja (Ed.), Damage Mechanics of Composite Materials, Elsevier, Amsterdam 1994, pp. 1–51.
[7] S. Andrieux, Y. Bamberger, J.-J. Marigo, Un modèle de matériau microfissuré pour les bétons et les roches, J. Méc. Théor. Appl. 5 (1986) 471–513.
[8] L. Gambarotta, S. Lagomarsino, A microcrack damage model for brittle materials, Int. J. Solids Structures 30 (1993) 177–198.
[9] C. Fond, Y. Berthaud, Extensions of the pseudo tractions technique for friction in cracks, circular cavities and external boundaries; effect of the interactions on the homogenized stiffness, Int. J. Fracture 74 (1995) 1–28.
[10] B.R. Lawn, D.B. Marshall, Nonlinear stress–strain curves for solids containing closed cracks with friction, J. Mech. Phys. Solids 46 (1998) 85–113.
[11] A. Dragon, F. Cormery, T. Désoyer, D. Halm, Localised failure analysis using damage models, in: R. Chambon, J. Desrues, I. Vardoulakis (Eds.), Localization and Bifurcation Theory for Soils and Rocks, A.A. Balkema, Rotterdam, 1994, pp. 127–140.
[12] D. Halm, A. Dragon, A model of anisotropic damage by mesocrack growth; unilateral effect, Int. J. Damage Mech. 5 (1996) 384–402.
[13] D. Halm, A. Dragon, An anisotropic model of damage and frictional sliding for brittle materials, Euro. J. Mech. A/Solids 17 (1998) 439–460.
[14] M. Kachanov, Effective elastic properties of cracked solids: critical review of some basic concepts, Appl. Mech. Rev. 45 (1992) 304–335.
[15] M. Ortiz, An analytical study of the localized failure modes of concrete, Mech. Mat. 6 (1987) 159–174.
[16] R. Billardon, I. Doghri, Localization bifurcation analysis for damage softening elastoplastic materials, in: J. Mazars, Z.P. Bazant (Eds.), Cracking and Damage, Strain Localization and Size Effect, Elsevier, London, 1989, pp. 295–307.
[17] T. Desoyer, F. Cormery, On uniqueness and localization in elastic-damage materials, Int. J. Solids Struct. 31 (1994) 733–744.
[18] S. Govindjee, G.J. Kay, J.C. Simo, Anisotropic modelling and numerical simulation of brittle damage in concrete, Int. J. Numer. Meth. Engrg. 38 (1995) 3611–3633.
[19] G. Pecqueur, A. Mikolajczak, J.M. Siwak, A. Dragon, Validation of an anisotropic damage model under torsional loading, in: G. Barla (Ed.), EUROCK'96, vol. 1, Prediction and Performance in Rock Mechanics and Rock Engineering, A.A. Balkema, Rotterdam, 1996, pp. 11–18.
[20] G. Pecqueur, Etude expérimentale et modélisation du comportement d'une craie et d'un grès en torsion, Doctoral Thesis, University of Lille I, 1995.
[21] Z. Wesolowski, Elastic material with different elastic constants in two regions of variability of deformation, Arch. Mech. 21 (1969) 449–468.
[22] A. Curnier, Q. He, P. Zysset, Conewise linear elastic materials, J. Elasticity 37 (1995) 1–38.
[23] R. Michalowski, Z. Mroz, Associated and non-associated sliding rules in contact friction problems, Arch. Mech. 30 (1978) 259–276.
[24] A. Curnier, A theory of friction, Int. J. Solids Struct. 20 (1984) 637–647.
[25] H. Horii, S. Nemat-Nasser, Compression-induced microcrack growth in brittle solids: axial splitting and shear failure, J. Geophys. Res. 90 (1985) 3105–3125.
[26] F. Cormery, Contribution à la modélisation de l'endommagement par mésofissuration et du phénomène de localisation associé, Doctoral Thesis, University of Poitiers and ENSMA, 1994.
[27] M. Ortiz, E.P. Popov, Accuracy and stability of integration algorithms for elastoplastic constitutive relations, Int. J. Num. Meth. Engrg. 21 (1985) 1561–1576.
[28] D.V. Pham, Suivi numérique des bandes de localisation dans les structures endommageables (endommagement par mésofissuration, anisotropie induite). Applications en géomécanique, Doctoral Thesis, University of Poitiers and ENSMA, 1994.
[29] D. Halm, Contribution à la modélisation du comportement unilatéral et du frottement dans les matériaux mésofissurés, Doctoral Thesis, University of Poitiers and ENSMA, 1997.